Article

Duplication of *NRAMP3* gene in poplars generated two homologous transporters with distinct functions

Mathieu Pottier[1,3], *Van Anh Le Thi*[1,4], *Catherine Primard-Brisset*[1], *Jessica Marion*[1], *Michele Bianchi*[1], *Cindy Victor*[1], *Annabelle Déjardin*[2], *Gilles Pilate*[2], *Sébastien Thomine*[1]*

[1]Institut de Biologie Intégrative de la Cellule, CNRS, Avenue de la Terrasse, 91198 Gif-sur-Yvette, France

[2]INRAE, ONF, BioForA, Orléans, France

[3]Current affiliation: Institute for Molecular Physiology, Heinrich-Heine-University Düsseldorf, Düsseldorf 40225, Germany

[4]Current affiliation: Graduate University of Science and Technology (GUST), Vietnam Academy of Science and Technology (VAST), 18 Hoang Quoc Viet, Cau Giay, Hanoi 10000, Vietnam

*Author for correspondence

Sébastien Thomine

Sebastien.thomine@i2bc.paris-saclay.fr

ABSTRACT

Transition metals are essential for a wealth of metabolic reactions, but their concentrations need to be tightly controlled across cells and cell compartments, as metal excess or imbalance has deleterious effects. Metal homeostasis is achieved by a combination of metal transport across membranes and metal binding to a variety of molecules. Gene duplication is a key process in evolution, as emergence of advantageous mutations on one of the copies can confer a new function. Here, we report that the poplar genome contains two paralogues encoding NRAMP3 metal transporters localized in tandem. All *Populus* species analyzed had two copies of *NRAMP3*, whereas only one could be identified in *Salix* species indicating that duplication occurred when the two genera separated. Both copies are under purifying selection and encode functional transporters, as shown by expression in the yeast heterologous expression system. However, genetic complementation revealed that only one of the paralogues has retained the original function in release of metals stored in the vacuole previously characterized in *A. thaliana*. Confocal imaging showed that the other copy has acquired a distinct localization to the Trans Golgi Network (TGN). Expression in poplar indicated that the copy of NRAMP3 localized on the TGN has a novel function in the control of cell-to-cell transport of manganese. This work provides a clear case of neo-functionalization through change in the subcellular localization of a metal transporter as well as evidence for the involvement of the secretory pathway in cell-to-cell transport of manganese.

Keywords: manganese, metal, recycling, Golgi apparatus, vacuole, Arabidopsis, *Salix*, *Populus*, selective pressure, evolution, apoplasmic transport, symplasmic transport, nutrition, micronutrient.

INTRODUCTION

Several transition metals are essential cofactors for a wealth of metabolic reactions in all living organisms. Iron (Fe) and copper (Cu) are for example needed in large amounts for the respiratory electron transfer chains and ATP production in bacteria and mitochondria. Transition metals are also important for DNA synthesis, proteolysis and the control of reactive oxygen species (ROS). Photosynthetic organisms have an additional specific requirement for manganese (Mn) for light energy conversion and water splitting (Shen 2015). Although they

are essential, transition metal concentrations need to be tightly controlled across cells and cell compartments, as excess or imbalance between different metals has deleterious effects. Metal homeostasis is achieved by a combination of metal transport across membranes and metal binding to a variety of molecules, including proteins, small peptides, amino acids, organic acids and more specialized metabolites, such as phytochelatins or nicotianamine in plants (Seregin and Kozhevnikova 2020).

Many families of transporters are implicated in the maintenance of metal homeostasis, either for metal uptake, distribution of metals to organs within organisms and organelles within a cell, or for removal and sequestration of excess metal. For example, in *Arabidopsis thaliana*, Mn is taken up by AtNRAMP1 (Natural Resistance Associated Macrophage Protein 1) in the roots and distributed within cells by AtNRAMP2 (Cailliatte et al. 2010; Alejandro et al. 2017; Gao et al. 2018). AtMTP8 (Metal Tolerance Protein 8) and AtMTP11, which belong to a different transporter family, are responsible for loading Mn from the cytosol into the vacuole or the Trans Golgi Network (TGN), respectively (Delhaize et al. 2007; Peiter et al. 2007; Eroglu et al. 2016). The vacuole is used to store Mn excess and prevent its toxicity. However, when this element becomes scarce, other NRAMP family members, namely AtNRAMP3 and AtNRAMP4, allow the retrieval of Mn from the vacuole (Lanquar et al. 2010). Mn is needed in the secretory system as a cofactor of glycosyl transferases involved in protein glycosylation (Alejandro et al. 2020). It also plays important roles as a cofactor of Super Oxide Dismutase in mitochondria and peroxisomes (Alejandro et al. 2020). Moreover, Mn is essential for oxygenic photosynthesis as a component of the Mn_4CaO_5 cofactor of the water splitting complex, which is bound to photosystem II (PS II) at the inner side of the thylakoid membranes (Shen 2015). CMT1 (Chloroplast Manganese Transporter 1) and PAM71 (Photosynthesis-affected mutant 71), two transporters belonging to the GDT1 family, have been shown to allow the import of Mn across the inner membrane of the chloroplast envelope and the thylakoid membrane, respectively (Schneider et al. 2016; Eisenhut et al. 2018; Zhang et al. 2018). Recently, another member of the GDT1/UPF0016 family was shown to play a crucial role in loading Mn in the Golgi apparatus, where it is needed as a cofactor of glycosyl transferases involved in cell wall formation (Yang et al. 2021). The networks of transporters that mediate uptake, storage and distribution of other essential metals, such as Fe, Zn and Cu, have also been described. Interestingly, these networks are interconnected, as some transporters, as well as ligands, are able to transport a broad range of metal cations (Mathieu Pottier et al. 2015b; Seregin and Kozhevnikova 2020).

This is well illustrated when looking at the functions of transporters of the NRAMP family. This family was first identified in the context of resistance to intracellular pathogens, such *Mycobacterium tuberculosis*, in mammals. Murine NRAMP1 was shown to limit the growth of intracellular pathogens by depleting essential metals from the phagosomes where they reside (Vidal et al. 1993; Wessling-Resnick 2015). Mammalian NRAMP2 plays a central role in Fe absorption in the intestine and recycling. In yeast, the NRAMP members SMF1 and SMF2 are involved in Mn absorption and distribution, similar to *A. thaliana* NRAMP1 and NRAMP2 (Portnoy et al. 2000; Cailliatte et al. 2010; Alejandro et al. 2017; Gao et al. 2018), while SMF3 allows the release of Fe from the vacuole, similar to *A. thaliana* NRAMP3 and NRAMP4 (Portnoy et al. 2000; Lanquar et al. 2005). In *A. thaliana*, NRAMP1 does not only allow high affinity Mn uptake but also plays a role in low affinity Fe uptake (Castaings et al. 2016). Besides Fe, AtNRAMP3 and AtNRAMP4 also allow the release of Mn from the vacuoles (Lanquar et al. 2005; Lanquar et al. 2010), clearly illustrating that these transporters connect Fe and Mn homeostasis.

While many studies have addressed the molecular mechanisms of metal homeostasis in *A. thaliana* and rice, there are only a limited number of reports on this topic in poplar. Poplars are both a model trees for which the genome of several species has been sequenced (Tuskan et al 2006; Zhang et al. 2019, Lin et al. 2018), and an industrially important crop for wood production. Poplars display outstanding growth yield among tree species and their wood is mostly used by the peeling industry to produce light packaging and plywood. Moreover, poplars are often used in the rehabilitation of polluted areas because it is highly tolerant to heavy metals and other contaminants (Krämer 2005a; Pottier et al. 2015a). Poplar MTP family members have been functionally investigated. In the first sequenced poplar species *Populus trichocarpa* (Tuskan et al., 2006), it has been shown that PotriMTP1 and PotriMTP11 could be the functional homologues of AtMTP1 and AtMTP11 and are involved in Zn loading into the vacuole and Mn loading into the TGN, respectively (Blaudez et al. 2003; Kramer 2005b; Peiter et al. 2007). Copper homeostasis has also been investigated in the context of photosynthetic efficiency (Ravet et al. 2011). In addition, overexpression of genes involved in Zn and Cd chelation and homeostasis has been undertaken in an attempt to increase tolerance and accumulation of these metals (Adams et al. 2011; He et al. 2015; Wang et al. 2019). Several studies have mined poplar genomic data and established lists of metal transport proteins in this species, analyzed the expression pattern of the corresponding genes and sometimes demonstrated the transport function using yeast complementation (Migeon et al. 2010; Li et al. 2015; Gao et al. 2020).

These studies have often highlighted the presence of duplication in metal homeostasis genes, which is a prevalent feature in poplar genome (Tuskan and et al 2006). However, they have not investigated in detail the function of the duplicated copies.

Gene duplication is a key process in evolution. It occurs through two major processes: either whole genome duplication or local duplication by inequal cross over or transposition (Conant and Wolfe 2008). Gene duplication underlies several key events in evolution such as variation in gene copy number, the generation of new regulatory networks and the appearance of novel functions. After gene duplication occurs, relaxation of selective pressure opens the door to several scenarios. Most of the time, one of the copies undergoes non-functionalization through accumulation of deleterious mutations due to the lack of selective pressure on this copy. In other cases, having multiple copies of the same gene provides advantages and several functional identical genes are therefore actively maintained (Hanikenne et al. 2013). Often the copies can also undergo sub-functionalization: the preduplication function is maintained but partitioned among the two copies. Typically, the expression pattern of the ancestral gene is covered by the two copies which are expressed in different organs and involved in distinct regulatory networks (Tuskan and et al 2006). Finally, in rare cases, emergence of advantageous mutations on one of the copies can also confer a new function, which is commonly known as neo-functionalization (Moriyama et al. 2016).

In this study, we have investigated the function of poplar *NRAMP3*. We found that the poplar genome contains two paralogues of *NRAMP3* in tandem. One of the paralogues has conserved the original function in release of metals stored in the vacuole characterized in *A. thaliana*, whereas the other paralogue has acquired a distinct localization to the TGN. Analysis of the function of this gene in transgenic poplars indicates that it has a novel function in the control of cell-to-cell transport of Mn in this species. Therefore, the functional analysis of the two paralogues of *PotriNRAMP3* provides a clear case of neo-functionalization through change in the subcellular localization of a transporter and evidence for the involvement of the secretory pathway in cell-to-cell transport of Mn.

RESULTS

PotriNRAMP3.1 and *PotriNRAMP3.2* are a tandem gene pair encoding homologous proteins

Plant NRAMPs are distributed into three different phylogenetic groups according to their protein sequence identities and exon-intron structures (Migeon et al. 2010). The eleven NRAMPs retrieved from *P. trichocarpa* genome V4.1 follow the same distribution (supplementary tables S1, S2 and fig. S1A). PotriNRAMP1, PotriNRAMP6.1 and PotriNRAMP6.2 as well as PotriNRAMP7.1, PotriNRAMP7.2 and PotriNRAMP7.3 belong to group I, which also includes AtNRAMP1 and AtNRAMP6. PotriNRAMP2, PotriNRAMP3.1 and PotriNRAMP3.2 are in group II, which includes AtNRAMP2, AtNRAMP5, AtNRAMP3 and AtNRAMP4. PotriEIN2.1 and PotriEIN2.2 are located in the group III as AtEIN2 (supplementary fig. S1A).

Interestingly, *PotriNRAMP3.1* and *PotriNRAMP3.2* genes are localized in close vicinity in *P. trichocarpa* genome. They are positioned in a 32 kb area of chromosome 7 and encode 88.2% identical proteins (supplementary fig. S1B-C). Dot plot analyses performed on genomic DNA including *PotriNRAMP3.1* and *PotriNRAMP3.2* genes show similarity specifically between their coding sequences and their 3'UTR but not between their introns and the surrounding genomic sequences (supplementary fig. S1C-D).

NRAMP3.1 **and** ***NRAMP3.2*** **are present in all sequenced poplar species but not in closely related species**

To determine how widespread the duplication of *NRAMP3* observed in *P. trichocarpa* genome is, sequences similar to *PotriNRAMP3.1* and *PotriNRAMP3.2* were retrieved from nine genomes and four transcriptomes and *Populus* species, covering the five main *Populus* sections, *i.e.*, Tacahamaca, Populus, Leucoïdes, Turanga, Aigeiros and Abaso (Zhang et al. 2019; Wang et al. 2020). We could unequivocally identify two distinct sequences similar to *PotriNRAMP3.1* or *PotriNRAMP3.2*, in all investigated *Populus* genomes, *i.e.*, *P. alba, P. cathayana, P. simonii, P. lasiocarpa, P. maximowiczii, P. euphratica, P. ussuriensis, P. nigra, P. deltoides, P. tremula, P. tremuloides* and *P. grandidentata* (supplementary table S1 and supplementary data S1) (Zhang et al. 2019). Evidence for two distinct sequences similar to *PotriNRAMP3.1* or *PotriNRAMP3.2* was also observed in *P. mexicana*, the single living species of the ancestral poplar section Abaso, even though its genome is not fully sequenced yet (supplementary table S1 and data S2) (Wang et al. 2020). This result suggests that distinct *PotriNRAMP3.1* and *PotriNRAMP3.2* homologues are present in all *Populus* species. In contrast, reciprocal blasting of *PotriNRAMP3.1* and *PotriNRAMP3.2* on the genome sequences of three Salix species (*S.*

purpurea, S. suchowensis and S. brachista), and on transcript sequences of five other Salix species (*S. viminalis, S. sachalinensis, S. eriocephala, S. fargesii* and *S. dasyclados)* that belong to the closest phylogenic group to *Populus* genus, identified a single sequence similar to *NRAMP3* in each species (supplementary table S1 and data S1) (Chen et al. 2019). These results suggest that the duplication that gave rise to *NRAMP3.1* and *NRAMP3.2* genes coincided with the divergence between *Populus* and *Salix* about 52 million years ago (Ma) (Hou et al. 2016). However, the chromosomal rearrangements that distinguish *Populus* and *Salix* phylum did not affect chromosome 7, which carries the *NRAMP3* loci (Hou et al. 2016). Moreover, gene collinearity is maintained around *NRAMP3* loci in *P. trichocarpa* and *S. purpurea* (fig. 1). Using the corresponding protein sequences of all the *Populus* and *Salix* NRAMP3 homologues identified during this analysis (supplementary data S3), we constructed a detailed phylogenetic tree. The *A. thaliana* NRAMP2, NRAMP3 and NRAMP4, and *P. trichocarpa* and *S. purpurea* homologues of AtNRAMP2 were used as outgroup (supplementary table S3). This analysis showed that *Populus* NRAMP3.1 and NRAMP3.2 protein sequences form distinct phylogenetic groups (fig. 2). The *Salix* homologues clearly cluster together with *Populus* NRAMP3.2 suggesting that it corresponds to the ancestral copy, whereas *Populus* NRAMP3.1 sequence diverged.

To further analyze the evolutionary history of *Populus* NRAMP3.1 and NRAMP3.2 sequences, we calculated the ratio of non-synonymous (dN) vs synonymous codons (dS), between all NRAMP3.1s, between all NRAMP3.2s, and between all NRAMP3.1s and NRAMP3.2s together. Low global dN/dS around 0.2 were obtained for NRAMP3.1 and NRAMP3.2 indicating that all genes are under purifying selection. A sliding window analysis revealed that the low global dN/dS values obtained among NRAMP3.1 or among NRAMP3.2 sequences result from homogeneously low ratios values along their open reading frames (supplementary fig. S2). In contrast, comparing NRAMP3.1s with NRAMP3.2s revealed heterogeneous values along the open reading frame, with ratios above or close to 1 in the N and C termini, as expected from divergent sequences. These results indicate that relaxation of selective pressure led to sequence diversity after the duplication event, but that both genes are now under purifying selection. Fixed Effects Likelihood (FEL) method was then employed to investigate site specific selective pressures specifically applied to either NRAMP3.1s or NRAMP3.2s. In this way, 21 and 4 residues under purifying selection ($p < 0.05$) were identified in NRAMP3.1s and NRAMP3.2s, respectively (supplementary tables S4 and S5). These residues are highlighted on an alignment between the consensus sequence of *Populus* NRAMP3.1 and that of *Populus*

NRAMP3.2 generated from all the *Populus* NRAMP3.1 and NRAMP3.2 sequences retrieved in this study (fig. 3; supplementary data S1 and fig. S3). Note that the four residues under purifying selection in NRAMP3.2s are also under purifying selection in NRAMP3.1s. Moreover, with the exception of V491, amino acids under purifying selection in NRAMP3.1s are conserved in NRAMP3.2s. These results suggest essential roles of these residues in the basal NRAMP3 function, common to both NRAMP3.1 and NRAMP3.2. In contrast, distinct residues were found to be under positive selection in both NRAMP3.1 (positions 3 and 437, $p < 0.05$) and NRAMP3.2 (positions 161 and 265, $p < 0.05$) (fig. 3; supplementary tables S4 and S5). Thus, NRAMP3.1 and NRAMP3.2 sequences both continue to diversify, even though they are globally under strong purifying selection. Moreover, these analyses indicate that NRAMP3.1 and NRAMP3.2 are not under non-functionalization.

Both *PotriNRAMP3.1* and *PotriNRAMP3.2* encode functional metal transporters

We then went on to examine the functions of the two paralogues. We cloned the corresponding cDNAs from *P. trichocarpa* and expressed them in yeast. Since their *A. thaliana* closest sequence homologues AtNRAMP3 and AtNRAMP4 are involved in Mn transport, we investigated PotriNRAMP3s ability to complement the *smf1* strain, which is deficient in Mn uptake (Supek et al. 1996). The *smf1* yeast strain fails to grow on synthetic medium containing high concentrations of the divalent cation chelator EGTA unless it is supplemented with Mn (Supek et al. 1996; Cohen et al. 2000). Expression of *PotriNRAMP3.2* restored the ability of *smf1* to grow on EGTA to the same extent as the positive control *AtNRAMP1* (Thomine et al. 2000). In contrast, PotriNRAMP3.1 complemented *smf1* phenotype with lower efficiency (fig. 4A; supplementary fig. S4). This result may be due to lower expression of *PotriNRAMP3.1* compared to *PotriNRAMP3.2* in yeast, a different subcellular localization or a lower efficiency of Mn transport. To test the hypothesis that a different localization accounts for the poor complementation of *smf1* by PotriNRAMP3.1, we complemented *smf2*, a yeast strain lacking an intracellular NRAMP involved in Mn supply to mitochondria and Golgi (Cohen et al. 2000; Luk and Culotta 2001). As *smf1*, this strain is unable to grow on high EGTA unless Mn is supplemented. We found that both PotriNRAMP3.1 and PotriNRAMP3.2 fully complement the *smf2* phenotype as efficiently as the positive control AtNRAMP2 (fig. 4B; supplementary fig. S5) (Alejandro et al. 2017). Moreover, the exposure to toxic Mn concentration in the absence of EGTA decreased the growth of the *smf2* strains transformed by *AtNRAMP2, PotriNRAMP3.1*

and *PotriNRAMP3.2* whereas it did not strongly affect the growth of *smf2* transformed by *GUS* (fig. 4B; supplementary fig S5). This increase of sensitivity to Mn was more pronounced for PotriNRAMP3.1. To further analyze their ability to transport Mn, cation accumulation was measured in *smf2* yeast expressing *AtNRAMP4*, *PotriNRAMP3.1* or *PotriNRAMP3.2*. Consistent with their ability to complement yeast Mn transport mutants (Thomine et al. 2000), Mn concentration was higher in yeast expressing *AtNRAMP4* as a positive control, or *PotriNRAMP3.1* and *PotriNRAMP3.2* compared to yeast expressing *GUS* as a negative control. This result confirms that both PotriNRAMP3.1 and PotriNRAMP3.2 proteins are able to transport Mn (fig. 4C).

As their *A. thaliana* closest sequence homologues AtNRAMP3 and AtNRAMP4 are also able to transport Fe, we tested the ability of PotriNRAMP3.1 and PotriNRAMP3.2 to complement the *fet3fet4* strain, which is deficient for both low- and high-affinity Fe uptake systems and requires a high Fe concentration for growth (Eide et al. 1996). Expression of *AtNRAMP4* and to a lesser extent that of *AtNRAMP1* were previously shown to restore *fet3fet4* growth on a low Fe medium (Thomine et al. 2000). We found that expression of *PotriNRAMP3.1* and *PotriNRAMP3.2* rescues *fet3fet4* growth under Fe limitation at a level intermediate between AtNRAMP4 and AtNRAMP1, indicating that they are both able to transport Fe (fig. 5; supplementary fig. S6).

Taken together, this work shows that both copies of PotriNRAMP3 have retained Mn and Fe transport ability, definitively excluding non-functionalization. Besides, these results also suggest that these two proteins have distinct subcellular localizations.

***NRAMP3.1* and *NRAMP3.2* are both expressed in poplar roots, stems, leaves and buds**

To test whether *Populus NRAMP3.1* and *NRAMP3.2* had undergone sub-functionalization by expression in distinct organs, their transcript levels were determined using RT-qPCR, in roots, stems, buds and leaves of the poplar hybrid INRA 717-1-B4 (*P. tremula* x *P. alba*)(Leplé et al. 1992). We designed primers that allow specific amplification of *NRAMP3.1* or *NRAMP3.2*, (supplementary table S6). *Populus NRAMP3.1* and *NRAMP3.2* exhibited expression in all studied organs (fig. 6). *NRAMP3.2* mRNA level was overall higher than that of *NRAMP3.1*. *NRAMP3.1* mRNA level was similar in all organs, whereas that of *NRAMP3.2* was higher in stems and leaves compared to roots and buds. These results show that, in the conditions tested,

NRAMP3.1 and *NRAMP3.2* are both expressed in all tested organs, arguing against their subfunctionalization by expression in distinct organs of the plants.

PotriNRAMP3.2*, but not *PotriNRAMP3.1*, complements the *nramp3nramp4* double mutant of *A. thaliana

Because both PotriNRAMP3s share high protein sequence identity with AtNRAMP3 and AtNRAMP4, we tested whether they could perform the same function *in planta*. AtNRAMP3 and AtNRAMP4 have redundant function in iron remobilization from vacuoles during seed germination. As a consequence, *A. thaliana nramp3nramp4* double mutants are sensitive to iron starvation during their early development (Lanquar et al. 2005). We expressed *PotriNRAMP3.1* and *PotriNRAMP3.2* under the *Ubiquitin 10* (*pUb10*) promoter in the *A. thaliana* Columbia 0 (Col-0) *nramp3nramp4* mutant background (Lanquar et al. 2005; Oomen et al. 2009; Grefen et al. 2010), and used 3 independent homozygous T3 lines expressing transgenes at various levels for further experiments (supplementary fig. S7). After eight days of growth under Fe starvation, lines transformed with *pUb10:PotriNRAMP3.2* exhibited full complementation of the double mutant phenotype: root length and cotyledon greening were indistinguishable from wild-type (fig. 7). Complementation was observed irrespective of the expression level of the transgene, indicating that even low levels are sufficient to restore the wild-type phenotype. In contrast, the expression of *PotriNRAMP3.1* did not improve the growth of the *A. thaliana nramp3nramp4* double mutant under Fe deficient conditions, even in lines showing high expression of the transgene (fig. 7, supplementary fig. S7). Similar results were obtained with the *p35S:PotriNRAMP3.1-GFP* and *p35:PotriNRAMP3.2-GFP* constructs used to study subcellular localization in both *A. thaliana* and poplar (see below), except that *p35S:PotriNRAMP3.1-GFP* partially improved *nramp3nramp4* growth under Fe deficiency (supplementary fig. S8). Even though PotriNRAMP3.1 is able to transport Fe (fig. 5), it is thus not able to restore Fe remobilization during seed germination.

PotriNRAMP3.1 and PotriNRAMP3.2 have distinct subcellular localizations in plant cells

Change in intracellular localization is one of the mechanisms leading to neofunctionalization (Ren et al. 2014). Because *smf1* complementation results suggest that PotriNRAMP3.1 and

PotriNRAMP3.2 may have distinct subcellular localizations (fig. 4), *A. thaliana* and poplar transgenic lines expressing C-terminal GFP fusion proteins of these two transporters were generated. Previous studies showed that tagging with GFP at the C-terminal end does not affect NRAMP targeting and function in plants (Lanquar et al. 2005; Cailliatte et al. 2010; Alejandro et al. 2017). The *A. thaliana nramp3nramp4* double mutant (Col-0) was stably transformed with *p35S:PotriNRAMP3.1-GFP* and *p35S:PotriNRAMP3.2-GFP*. Roots of these plants were then observed by confocal microscopy (fig. 8). Interestingly, distinct subcellular localizations were observed for PotriNRAMP3.1-GFP and PotriNRAMP3.2-GFP. While PotriNRAMP3.2-GFP was targeted to the vacuolar membrane, as its homologues in *A. thaliana* and *Noccaea caerulescens* (Thomine et al. 2003; Lanquar et al. 2005; Oomen et al. 2009), PotriNRAMP3.1 was localized in intracellular punctuate structures (fig. 8). The localization of PotriNRAMP3.2 on the vacuolar membrane is consistent with its ability to complement the *A. thaliana nramp3nramp4* double mutant. Similar PotriNRAMP3.1 and PotriNRAMP3.2 localizations were observed in poplar root cells (fig. 8) as well as in mesophyll protoplasts and leaf epidermal cells (supplementary fig. S9).

To determine more precisely the subcellular localization of PotriNRAMP3.1, we tested the colocalization of PotriNRAMP3.1-GFP with RFP markers for different cell compartments (Ebine et al. 2011; Uemura et al. 2012; Inada et al. 2016). To this aim, *A. thaliana* lines expressing PotriNRAMP3.1-GFP were crossed with stable lines expressing markers for the trans Golgi apparatus *i.e.*, mRFP-ST (Sialyl Transferase), the TGN *i.e.*, mRFP-Syp43 and two endosomal markers *i.e.*, ARA6-mRFP and ARA7-mRFP. Spinning disk confocal microscopy performed on the F1 seedlings showed an extensive overlap between PotriNRAMP3.1-GFP and mRFP-SYP43 fluorescence (fig. 9A). Interestingly, although PotriNRAMP3.1-GFP fluorescence did not overlap with that of mRFP-ST, it was most often in close vicinity (fig. 9B). In contrast, little or no colocalization was observed with endosomal markers (supplementary fig. S10). These colocalization experiments indicate that PotriNRAMP3.1 resides on the TGN, and that it is present in both Golgi-associated and Golgi-independent TGN compartments (Viotti et al. 2010; Uemura et al. 2019). Together, these results show that the *PotriNRAMP3.2* copy has retained the subcellular localization and function of the *NRAMP3* genes characterized in other species, whereas *PotriNRAMP3.1* has likely acquired a novel function due to mutations that modified its subcellular localization to the TGN. However, *PotriNRAMP3.1* expression in *A. thaliana* did not lead to any phenotypic alteration that could provide hints at this novel function.

342

343 **PotriNRAMP3.1, but not PotriNRAMP3.2, affects manganese homeostasis in poplar**

344 To investigate the functions of PotriNRAMP3.1 and PotriNRAMP3.2 in poplar, the genes
345 coding these transporters were over-expressed as GFP fusions under the control of the CaMV
346 35S promoter. For each construct, four independent transgenic lines overexpressing (OE) the
347 *PotriNRAMP3s* at levels 10 to 40 times higher than non-transgenic (NT) control trees were
348 analyzed (supplementary fig. S11). Their physiological characterization highlighted that poplar
349 lines with the highest levels of *PotriNRAMP3.1* expression displayed reduced height as well as
350 interveinal chlorosis on mature leaves compared to NT control trees (fig. 10A, C, F;
351 supplementary fig. S11). In contrast, *PotriNRAMP3.2* OE trees were indistinguishable from NT
352 poplars (fig. 10B, C, H). To better understand the origin of the chlorosis, the maximum quantum
353 yield of PS II was imaged using an Imaging PAM (Walz, Germany) in leaves of control poplars
354 as well as *PotriNRAMP3.1* and *PotriNRAMP3.2* OE lines (fig. 10E, G, I). The chlorotic areas
355 in *PotriNRAMP3.1* OE lines coincided with strongly decreased PS II maximum quantum yield
356 (0.472±0.035). In contrast, PS II efficiency was close to the optimal value of 0.82 in leaves
357 from control (0.756±0.002) and *PotriNRAMP3.2* OE trees (0.751±0.008). As interveinal
358 chlorosis is a symptom of Fe deficiency and decrease in PS II efficiency may be a symptom of
359 Mn deficiency (Connorton et al. 2017; Alejandro et al. 2020), we quantified metals in young,
360 mature and senescent leaves from the different poplar genotypes. These analyses revealed that
361 Mn concentrations in young and mature leaves were significantly lower in PotriNRAMP3.1 OE
362 lines compared to NT control or PotriNRAMP3.2 OE lines (fig. 11A, B, C). In contrast, no
363 significant difference in Fe or Zn concentrations was detected among the different genotypes
364 (supplementary fig. S12). Interestingly, opposite to what was observed in leaves, Mn
365 concentrations in stems of PotriNRAMP3.1 OE lines were higher than in NT control or
366 PotriNRAMP3.2 OE lines (fig. 11D). Note that Mn concentrations were also significantly
367 higher in stems of PotriNRAMP3.2 OE lines compared to NT control. The defect in Mn
368 distribution observed in PotriNRAMP3.1 OE lines suggests that the phenotypes observed in
369 these lines are due to a defect in Mn transfer from stems to leaves leading to limited Mn supply
370 to leaves.

371 To further test this hypothesis, we analyzed Mn distribution in mature leaves from
372 PotriNRAMP3.1 OE lines compared to NT control. We dissected leaves into vein and lamina,
373 and measured Mn separately (fig. 11E). In PotriNRAMP3.1 OE lines, the Mn concentration

was lower in lamina compared with veins, whereas the concentrations in these two parts of the leaf were similar in NT control. Moreover, the Mn concentration in the lamina was lower in PotriNRAMP3.1 OE lines than in the NT control line, while the opposite was observed in veins. These results confirm that overexpression of *PotriNRAMP3.1* in poplar perturbs Mn distribution between and within organs. This suggests that PotriNRAMP3.1 is involved in Mn transport between organs and tissues.

To confirm that the leaf chlorosis symptoms observed in PotriNRAMP3.1 OE lines were due to Mn depletion in the lamina, we supplemented the trees with Mn. We grew tree cuttings for 4 weeks and then started watering half of them with 0.5 mM of $MnSO_4$ for an additional 5 weeks. We observed that chlorosis did not appear in newly formed leaves of Mn treated trees (supplementary fig. S13A). In these leaves, Mn concentrations were higher in lamina and veins, but the treatment did not restore the defect in Mn distribution between these tissues (supplementary fig. S13B). Chlorosis was not reverted in leaves formed prior to the treatment indicating that the treatment prevented chlorosis in newly formed leaves rather than corrected it in older leaves.

Discussion

In this study, we have characterized two poplar metal transporter NRAMP3 using a combination of phylogenetic, cell biological and molecular genetic approaches. We found that poplar genomes harbor two tandem copies of NRAMP3 gene under selection, whereas only one copy is present in *Salix* genus, the closest phylum. Moreover, we demonstrated that the two paralogues encode functional metal transporters. However, they have acquired different functions *in planta*. Whereas PotriNRAMP3.2 has the same function in metal retrieval from the vacuole as AtNRAMP3 and AtNRAMP4, PotriNRAMP3.1 displays a distinct subcellular localization to the TGN as well as a distinct function. Our results show that PotriNRAMP3.1 is involved in Mn distribution in poplar aerial organs. Elemental analyses indicate that poplar lines ectopically expressing *PotriNRAMP3.1* are impaired in Mn transfer from the stem to the leaves and, within the leaves, from the vein to the lamina, resulting in chlorosis and a decreased PS II efficiency. Together our results show that a gene duplication of NRAMP3 specific to the poplar genus gave rise to the neofunctionalization of one of the copies, while the other retained the conserved function described in other species and highlight an unsuspected role of the secretory pathway in cell-to-cell transport of Mn.

406

407 **Distinct mechanisms for the formation of *NRAMP* gene pairs in *A. thaliana* and poplar**

408 Duplication events are a driving force in evolution, facilitating adaptation to changing
409 environments. Although gene duplication may be followed by accumulation of deleterious
410 mutations and gene elimination, it may also lead to diversification of gene function and sub- or
411 neo-functionalization (Yang et al. 2006). The ancestral angiosperm genome contained only
412 14000 genes or less (Proost et al. 2011). However, whole genome triplications occurring about
413 120 Ma, significantly increased the size of the Eudicotyledon genomes.

414 In *A. thaliana AtNRAMP3* and *AtNRAMP4* encode functionally redundant metal transporters
415 (Lanquar et al. 2005). This pair of genes located on two different chromosomes are present in
416 *A. thaliana*, *Arabidopsis lyrata* and *Noccea caerulescens* (Oomen et al. 2009), but not in *Carica*
417 *papaya* and *Ricinus communis* genomes. Thus, they probably originate from a duplication that
418 took place after the *Carica papaya* divergence that happened 72 Ma. The analysis of the
419 duplicated regions of the *A. thaliana* genome has showed that *AtNRAMP*3 and *AtNRAMP*4 loci
420 are located on the duplicated block 0204146800380, suggesting that the pair originates from
421 one of these two whole genome duplications that occurred between 70 and 23 Ma in the *A.*
422 *thaliana* lineage (Lanquar et al. 2005; Ming et al. 2008; Proost et al. 2011).

423 The poplar lineage has also undergone one whole genome duplication 60-65 Ma *i.e.*, before the
424 *Populus* and *Salix* divergence that took place 52 Ma (Tuskan and et al 2006; Hou et al. 2016).
425 Comparing gene order in *S. purpurea* and in *P. trichocarpa* showed genomic collinearity
426 upstream and downstream *NRAMP3 loci*, except that only one copy of *NRAMP3* is found in *S.*
427 *purpurea* (fig. 1). In contrast, two copies of *NRAMP3* were found in all sequenced poplar
428 genotypes (fig. 2). Thus, it is unlikely that this whole genome duplication account for the
429 emergence of *NRAMP3.1* and *NRAMP3.2* genes specific to *Populus* species since this event
430 happened before the *Populus* and *Salix* divergence. Moreover, gene tandem arrangements
431 generally imply local duplication processes rather than whole genome duplications. However,
432 the genomic sequence surrounding *Populus NRAMP3.1* and *NRAMP3.2* shows many remains
433 of Class I long terminal repeats (LTR) retrotransposon elements (Gypsy) mainly located
434 between the two genes. Retrotransposons can mediate gene duplications. However, such
435 duplications usually create a typical intron-free copy which can be integrated throughout the
436 genome and not specifically close to the initial copy (Freeling 2009). The conservation of
437 intron/exon structure and the tandem arrangement of *Populus NRAMP3.1* and *NRAMP3.2*

suggest another mechanism. Repeated sequences of retrotransposons are known to stimulate intrachromosomal recombination events or unequal crossing over, leading to gene duplication (White et al. 1994; Flagel and Wendel 2009). The genome of poplar which contains significantly more gene tandems than that of *A. thaliana* (Proost et al. 2011), contains also three time more transposons (Ming et al. 2008). Thus, it is most likely that this mechanism accounts for the tandem duplication of *Populus NRAMP3.1* and *NRAMP3.2*. Thus, distinct mechanisms of gene duplication led to *NRAMP* gene pair formation in poplar and *A. thaliana*.

Populus NRAMP3 copies are subjected to both positive and purifying selections

Most gene duplications are thought to be rapidly followed by the loss of function of one of the copies. This fate is referred as non-functionalization (Freeling 2009). While one paralogue retains the preduplication function, selective constraints generally relax on the second paralogue which, therefore, accumulates deleterious mutations leading to loss of function (Ohno 1970). However, pseudogene formation is not the only fate of duplicated genes. In few cases, both copies can retain function after a duplication event for different reasons. First, environmental conditions may maintain selective pressure on both genes to retain preduplication function, increasing fitness through dose effect. For example, multiple tandem copies of *HMA4* are maintained in the metal hyperaccumulator species *Arabidopsis halleri* and *N. caerulescens* leading to a high expression level essential for Zn and Cd translocation and metal tolerance (Ó Lochlainn et al. 2011; Craciun et al. 2012; Hanikenne et al. 2013).

Alternatively, relaxation of purifying selection allowed by gene duplication can also allow non-synonymous mutations while maintaining function in the two daughter genes. This can occur through two scenarios. One is the subfunctionalization, which is the partitioning of the preduplication function among daughter genes. The other one is the neofunctionalization which leads to the emergence of a new function in one of the gene copies, while preserving the sequence and the function of the ancestral gene in the other copy (Zhang 2003).

In the present study, dN/dS analysis highlights that *Populus NRAMP3.1* and *NRAMP3.2* sequences are mostly under purifying selection (fig. 3; supplementary tables S4 and S5) acting on many residues in the core conserved transmembrane domains of the protein. This is in agreement with the finding that both PotriNRAMP3.1 and PotriNRAMP3.2 have retained metal transport ability. However, they also exhibit a clear relaxation of purifying selection especially on residues localized at the N and C terminal ends of the protein (fig. 3; supplementary fig. S2,

tables S4 and S5). Mutations in the N terminal region, where motives involved in the targeting of AtNRAMP3 and AtNRAMP4 have previously been identified, likely enabled the protein to acquire distinct subcellular localizations (Müdsam et al. 2018). The vacuolar membrane localization of PotriNRAMP3.2 (fig. 8), its transport capacities (fig. 4, 5) and its ability to complement *A. thaliana nramp3nramp4* double mutant phenotypes (fig. 7) indicate that PotriNRAMP3.2 is the functional homologue of AtNRAMP3 and AtNRAMP4. The ability of PotriNRAMP3.1 to transport Fe and Mn in yeast (fig. 4, 5), its distinct intracellular localization (fig. 8, 9), its inability to complement the *nramp3nramp4* double mutant phenotypes (fig. 7) and the signature of purifying selection (fig. 3, supplementary fig. S2, tables S4 and S5) argue in favor of neo-functionalization rather than non-functionalization. The finding that *Populus NRAMP3.1* and *Populus NRAMP3.2* promoter sequences lack significant sequence identities further indicates that the regulation of the two copies has diverged (supplementary fig. S1D). This is in agreement with our previous report showing that *Populus NRAMP3.1* and *NRAMP3.2* belong to different networks of co-expressed genes (Pottier et al. 2015a). We propose a scenario in which after *Populus NRAMP3* gene duplication, relaxation of purifying selection allowed mutations altering PotriNRAMP3.1 subcellular localization. This mutated version of *Populus NRAMP3* was subsequently maintained by purifying selection, probably because it conferred improved fitness. Specific inactivation of *Populus NRAMP3.1* would allow to further test this scenario.

PotriNRAMP3.1 modulates tissue distribution of Mn

To investigate the function of these transporters *in planta*, we generated transgenic poplars over-expressing *PotriNRAMP3.1-GFP* and *PotriNRAMP3.2-GFP*. PotriNRAMP3.1 and PotriNRAMP3.2 subcellular localizations in poplar roots or leaves were similar to those observed in *A. thaliana*. (fig. 8, 9; supplementary fig. S9). Analysis of metal concentrations revealed a specific decrease in Mn concentrations in leaves from lines over-expressing *PotriNRAMP3.1-GFP*. Moreover, lines with the lowest Mn leaf concentrations displayed internerval chlorosis (fig. 10). In agreement with the role of Mn in photosynthesis, PS II efficiency was decreased in the chlorotic parts of *PotriNRAMP3.1* OE leaves (fig. 10). Further analysis showed that the decrease in Mn leaf concentration was associated to an increase in Mn concentration in stems (fig. 11). Furthermore, Mn distribution within leaves is also affected in *PotriNRAMP3.1* OE lines: Mn accumulates at higher levels in the veins while it is depleted in the lamina. Together, these results indicate that PotriNRAMP3.1 is involved in transcellular transport of Mn. This phenotype is unexpected as PotriNRAMP3.1-GFP exhibits a clear

intracellular localization to the TGN. To account with this phenotype, we propose a working model based on two hypotheses (1) Mn cell-to-cell transport requires Mn secretion (2) expression of *PotriNRAMP3.1* limits Mn secretion by allowing the retrieval of Mn from the TGN, which would otherwise be secreted. This model is illustrated in figure 12. The function of PotriNRAMP3.1 in retrieval of Mn from the secretory system is equivalent to the function of AtNRAMP2 (Alejandro et al. 2017; Gao et al. 2018). AtNRAMP2 localizes to the TGN and was proposed to retrieve Mn from this compartment to make it available for uptake into the chloroplasts. Previous work also showed that loss of AtMTP11, which also localizes in the secretory system, leads to an increase in plant Mn concentration (Peiter et al. 2007). As AtMTP11 is involved in Mn loading into the secretory system, the observed phenotype also agrees with the hypothesis that Mn concentrations in plant tissues are, at least in part, controlled by Mn secretion. As SMF2 has also been proposed to retrieve Mn from the secretory system in yeast, the proposed model would also account for the strong decrease in Mn content in the *smf2* mutant (Luk and Culotta 2001). Homologues of AtMTP11 and AtNRAMP2 are also present in poplar and could act in concert with PotriNRAMP3.1 to control the rate of Mn secretion vs intracellular distribution in poplar cells. Interestingly, mRNA levels of *PotriNRAMP2* and *PotriNRAMP3.1* are correlated in leaves (M. Pottier et al. 2015a).

Taken together, our results provide a clear case for neofunctionalization in a tandem of NRAMP genes specific to poplar. It also provides new insights into the cell-to-cell transport of divalent cations by showing the significant contribution of the secretory pathway in the cellular export of Mn. Besides, these results also provide new evidence of the essential role of transporters located at the secretory pathway in the regulation of the cellular storage of Mn. In the future, it would be interesting to find out what is the advantage conferred by the newly functionalized PotriNRAMP3.1 which led to the conservation of this gene in all examined poplar species. It will also be interesting to understand the interplay between PotriNRAMP3.1, PotriNRAMP2 and PotriMTP11 in the control of Mn concentration in the secretory pathway.

Materials and methods

Sequences analysis

Sequences were retrieved from Phytozome V13, PopGenIE V3, NCBI, TAIR and 1KP Project databases as indicated in the supplementary table S1 (Zhang 2003; Tuskan et al. 2006; Sjödin et al. 2009; Goodstein et al. 2012; Lamesch et al. 2012; Dai et al. 2014; Lin et al. 2018; Zhou

et al. 2018; Chen et al. 2019; One Thousand Plant Transcriptomes Initiative 2019; Sayers et al. 2021). To obtain the genomic sequence of *NRAMP3.1* (Potri007G050600) and *NRAMP3.2* (Potri007G050600) in *P. alba*, *P. cathayana, P. simonii, P. lasiocarpa, P. maximowiczii, P. euphratica, P. ussuriensis, P. nigra, P. deltoides*, and *P. mexicana*, raw reads were aligned to *P. trichocarpa* reference sequence V4.1 and the obtained genome consensus was blasted with *PotriNRAMP3.1* and *PotriNRAMP3.2* using QIAGEN CLC Genomics Workbench 12.0. *P. trichocarpa* and *S. purpurea* genomic DNA homologies were investigated by Dot-plot analyses performed on Gepard softwares V1.30 and V1.40 (Krumsiek et al. 2007).

Phylogenetic tree construction

Full-length amino acid sequences were aligned by CLUSTALW and imported into the Molecular Evolutionary Genetics Analysis (MEGA) package version 7 (Kumar et al. 2016). Phylogenetic analyses were conducted using the Maximum Likelihood method, based on the JTT matrix-based model (fig. 2) or Le_Gascuel (LG) model (supplementary fig. S1), implemented in MEGA7 (Jones et al. 1992; Le and Gascuel 2008). The bootstrap consensus tree inferred from 1000 replicates was taken to represent the evolutionary history of the analyzed genes. Branches corresponding to partitions reproduced in less than 50% bootstrap replicates were collapsed. Initial tree(s) for the heuristic search were obtained automatically by applying Neighbor-Joining and BioNJ algorithms to a matrix of pairwise distances estimated using a JTT model, and then selecting the topology with superior log likelihood value. A discrete Gamma distribution was used to model evolutionary rate differences among sites (5 categories, +*G*, parameter = 0.4725 and parameter = 1.2613 for figure 2 and supplementary figure S1, respectively). Trees are drawn to scale, with branch lengths measured in the number of substitutions per site. All positions with less than 95% and 90% site coverage were eliminated for figure 2 and supplementary figure S1, respectively.

Selective pressure analysis

To determine the nonsynonymous (dN) and synonymous (dS) substitution rates, and the dN/dS ratios along NRAMP3 coding sequence, pairwise comparisons were performed among the 13 *NRAMP3.1* sequences, among the 13 *NRAMP3.2* sequences, as well as between the 13 *NRAMP3.1* and the 13 *NRAMP3.2* sequences following codon based alignment using the

JCoDA v1.4 package with the Nei-Gojobori substitution model, with a 20 residue window and a shift of 10 residues (Nei, M and Gojobori, T 1986; Steinway et al. 2010). Positive and purifying selections at individual sites were subsequently inferred using the Fixed Effects Likelihood (FEL) method (Nei, M and Gojobori, T 1986; Steinway et al. 2010). The 26 NRAMP coding sequences were used to generate a phylogenetic tree. A subset of branches encompassing either the *NRAMP3.1s* or the *NRAMP3.2*s were analyzed separately to estimate dS and dN at a site (α and β, respectively). A maximum-likelihood approach was then undertaken to calculate the dN/dS for each codon site (ϖ; $p < 0.05$).

Gene expression

Total RNA from 1-month-old poplars or 1 week-old *A. thaliana* grown *in vitro* on half strength Murashige and Skoog (MS) or ABIS medium, respectively, was extracted using RNeasy Plant Mini Kit (Qiagen) as previously described (Pottier et al., 2015a). Five micrograms of DNA-free RNA were used for reverse transcription by the SuperScript III First-Strand kit (Invitrogen). Reverse transcriptions were performed using random hexamers. Gene-specific PCR primers were designed using OligoPerfect™ Designer (http://tools.lifetechnologies.com). All primers used for RT-qPCR are listed in supplementary table S6. One-sixth of the cDNAs was used as a template in 10-µl qPCR reactions performed on a Roche LightCycler 96 using Roche reagents, according to the manufacturer's instructions (http://www.roche.com). Primer specificity was confirmed by analysis of the melting curves and sequencing of the PCR products. Relative transcript levels were calculated by normalization to the transcript amount to constitutively expressed genes.

Construction of expression vectors.

PotriNRAMP3.1 and *PotriNRAMP3.2* CDSs were amplified by PCR from cDNA synthesized from leaf RNA of *P. trichocarpa* cv Nisqually-1. Primer PtNramp3aLgtw encompassing the ATG initiation codon was used with PtNramp3aRgtwstp encompassing the TAA stop codon or with PtNramp3aRgtwnostp designed before the TAA stop codon. Primer PtNramp3bLlonggtw encompassing the ATG initiation codon was used with PtNramp3bRlonggtwstp encompassing the TAA stop codon or with PtNramp3bRlonggtwnostp designed before the TAA stop codon. For *PotriNRAMP3.1*, amplification was performed in 2 steps, first with specific primers and

second using the generic U5 and U3 primers. Forward and reverse primers used for *NRAMP* cloning are shown in supplementary table S7. PCRs were performed with the Phusion high-fidelity DNA polymerase (Thermo-Scientific). The gel-purified PCR products were recombined into pDONR207 for *PotriNRAMP3.1* and into pDONR201 for *PotriNRAMP3.2* following the BP Clonase (Invitrogen) manufacturer's instruction.

For the generation of yeast expression vectors, LR reactions were performed using the pDR195gtw vector adapted to Gateway cloning (Rentsch et al. 1995; Oomen et al. 2009) and the pDONR (Invitrogen) containing *PotriNRAMP3.1* and *PotriNRAMP3.2* with stop codon.

For the generation of plant expression vectors, LR reactions, were performed to transfer *PotriNRAMP3s* fragments with or without stop codon from pDONR vectors to the Gateway binary over-expression vectors pB7WGF2, pB7FWG2 (Karimi et al. 2002) and pMDC83 (Curtis and Grossniklaus 2003) that contain the 35S CaMV promoter (p35S) and *GFP* sequence allowing to generate *PotriNRAMP3-GFP* fusion proteins. *PotriNRAMP3s* fragments with stop codon were also transferred in the pUB-DEST vector to drive their expression under control of Ubiquitin 10 promoter (Grefen *et al.* 2010).

Yeast strains, transformations and media

DEY1453 (*fet3fet4*, Eide *et al.* 1996), *smf1* (Supek, et al. 1996; Thomine, et al. 2000) and *smf2* (Cohen, et al. 2000) yeast strains were grown at 30ºC on Yeast extract/Peptone/Dextrose (before transformation) or synthetic dextrose -ura (after transformation). For the DEY1453 strain, media were supplemented with 0.2 mM $FeCl_3$. Yeast cells were transformed according to standard procedures (Invitrogen).

Yeast growth assays

Transformed *fet3fet4*, *smf1*, *smf2* yeast mutants were grown overnight in liquid synthetic dextrose -ura (pH 6) supplemented with 0.2 mM $FeCl_3$ for *fet3fet4* mutants. The cultures were diluted to ODs of 1 to 10^{-3} and spotted on synthetic dextrose-ura plates (pH 6). Transformed *fet3fet4* strains were spotted on media supplemented with 100 µM of the Fe chelator BathoPhenanthroline-Di-Sulfonic acid (BPDS) and 0.2 mM $FeCl_3$ (+ Fe) or with 100 µM BPDS and 40 µM $FeCl_3$ (-Fe). Transformed *smf1* strains were spotted on media supplemented with 5 mM ethylene glycol*bis*(beta-aminoethyl ether)-*N*,*N*,*N*′,*N*′-tetraacetic acid (EGTA) and 100 µM

628 $MnSO_4$ (+ Mn) or with 5 mM EGTA without $MnSO_4$ (- Mn). Transformed *smf2* strains were
629 spotted on media supplemented with 5 mM EGTA and 100 µM $MnSO_4$ (+ Mn), with 5 mM
630 EGTA without $MnSO_4$ (- Mn) or with 10 mM $MnSO_4$ (+++ Mn).

631

632 *Confocal imaging*

633 Roots of *in vitro* grown 6-day-old *A. thaliana* seedlings or 2-3 week-old poplar explants were
634 mounted in liquid culture medium, and confocal images of epidermal cells in the elongation
635 zone were obtained by high-speed (100 ms) sequential acquisition of GFP (λex = 490 nm, λem
636 = 500–550 nm) and mRFP (λex = 590 nm, λem = 600–650 nm, employing a Nipkow spinning
637 disk confocal system equipped with a Prime 95Bcamera (Photometrics) and a Nikon 100X 1.4
638 aperture oil immersion objective. Super resolution images were generated with a Live-SR
639 module for optically demodulated structured illumination (GATACA Systems). Image
640 processing (cropping, contrast adjustment and background subtraction) was performed with
641 ImageJ 1.45s program (Schneider et al. 2012).

642

643 *Plant material and plant transformation*

644 The generation of the *nramp3nramp4* double mutants of *A. thaliana* Col-0 was described
645 previously (Molins *et al.* 2012). *PotriNRAMP3.1* and *PotriNRAMP3.2* constructs were
646 introduced in Col-0 *nramp3nramp4* mutants through *A. tumefaciens* (strain AGL0) mediated
647 transformation using the flower dip method (Clough 2005). Independent homozygous *A.*
648 *thaliana* Col-0 *nramp3nramp4* transformants with a single insertion locus were obtained by
649 plant selection based on Basta resistance and complementation of the *nramp3nramp4*
650 phenotype on low Fe medium.

651 The poplar INRA 717-1-B4 clone (*P. tremula* x *P. alba*) was transformed as described (Leple
652 et al. 1992). Briefly, stem explants were excised from *in vitro* grown poplar and incubated for
653 2 days in the dark on M1 medium (Supplementary table S8). The explants were then co-
654 cultivated for 16 h at 24°C on an orbital shaker (180 rpm) with 150 ml of a suspension (OD
655 0.3) of *Agrobacterium tumefaciens* C58/pMP90 transformed with *p35S:PotriNRAMP3.1-GFP*
656 or *p35S:PotriNRAMP3.2-GFP* constructs in pMDC83. The explants were washed 5 times in
657 sterile water under orbital shaking (140 rpm). After washing, they were transferred on M2
658 medium containing Ticarpen, cefotaxime and hygromycin B, and incubated at 24°C in darkness

for 21 days (Supplementary table S8). The plates were subsequently transferred to light (16 h 130 µE.m^{-2}/8h dark) to recover green calli. The green calli were transferred to M3 agar medium with hygromycin B (Supplementary table S8). The regenerated transformed shoots were then transferred on half strength MS agar medium with hygromycin to allow root regeneration (Supplementary table S8). The transgenic lines were propagated on the same medium until transfer to pots in the greenhouse.

A. thaliana growth conditions

A. thaliana seedlings were grown on ABIS medium plates containing 2.5 mM H_3PO_4, 5 mM KNO_3, 2 mM $MgSO_4$, 1 mM $Ca(NO_3)_2$, MS microelements, 1% sucrose, 1% Phytagel, 1 mM MES adjusted with KOH to pH 6.1 and FeHBED (N,N'-di(2-hydroxybenzyl) ethylenediamine-N,N'diacetic acid monochloride hydrate; Strem Chemicals, Newburyport, MA, USA) as indicated in figure legends. FeHBED was prepared as described by Lanquar *et al*. (Lanquar, et al. 2005). For low iron sensitivity growth assays, plants were grown for 8 days on plates where Fe was omitted. Plates were placed vertically in environmental growth chambers (Sanyo MLR-350, Morigushi, Japan) at 21°C with a 16 h photoperiod under 120 µmol photon·m^{-2}·s^{-1}.

Photosystem II maximum quantum yield

Phostosystem II maximum quantum yield was determined using Imaging PAM (Walz, Germany). Efficiency of the photosynthetic electron transport (Fv/Fm) was assayed by calculating the ratio of variable fluorescence (Fv) to maximal fluorescence (Fm) after a saturating light pulse (Maxwell & Johnson 2000). Plants were dark adapted for 15 min prior to measurements. Five areas of interest (AOI) in the green part and 5 AOI in the chlorotic parts of each leaf were selected for quantification in three independent leaves of each genotype.

Root length measurements

Plants grown vertically on plates were photographed at the indicated times and root length was determined using the ImageJ 1.45s program and a digitizer tablet (WACOM Europe GMBH, Krefeld, Germany, Intuos 4M). Values are the average of measurements on 10–12 roots.

Metal concentration analysis

For metal analyses in yeast, liquid SD -ura medium containing transformed *smf2* strain growing overnight were diluted to OD 0.3 in liquid SD -ura supplemented with 30 µM $FeCl_3$ and 10 µM $MnSO_4$. After 30 h of incubation at 30°C under agitation, yeast cells were recovered by centrifugation (3340*g*, 5 min, 4°C) and washed twice in 50 ml ice cold YNB supplemented with EDTA 20 mM and MES 50 mM pH6, pelleted and then washed in ice cold ultrapure water.

For metal analyses in plants, shoots and roots were harvested separately and washed. Roots were desorbed by incubation in ice-cold buffer containing 5 mM $CaCl_2$ and 1 mM MES-KOH, pH 5.7, for 10 min.

The dry weight (DW) of the samples (yeasts or plants) was measured after drying at 60°C for 3 days. The dried samples were digested in 2 ml of 70 % nitric acid in a DigiBlock ED36 (LabTech, Italy) at 80°C for 1 h, 100°C for 1 h and 120°C for 2 h. After dilution in trace-metal-free water, the metal content of the samples was determined by atomic absorption spectrometry using an AA240FS flame spectrometer (Agilent, USA) or by atomic emission spectroscopy using a MP AES 1200 spectrometer (Agilent, USA).

Statistical analysis

Data were analyzed with Kruskal-Wallis and Mann-Whitney non-parametric tests for multiple comparisons and pair comparisons, respectively. For multiple comparisons, a Dunn's post hoc test was performed when significant differences were detected. Both tests were performed using GraphPad Prism 7.

Acknowledgments

This work was supported by grants from the DIM Astréa (Région Ile-de-France) to MP, from the VIED organisation to VALT and ANR PHYTOPOP (ANR-06-ECOT-0015) to ST. The authors thank Prof. Wolf B. Frommer for providing support.

715 **References**

716 Adams JP, Adeli A, Hsu C-Y, Harkess RL, Page GP, dePamphilis CW, Schultz EB, Yuceer
717 C. 2011. Poplar maintains zinc homeostasis with heavy metal genes HMA4 and PCS1. *J. Exp.*
718 *Bot.* 62:3737–3752.

719 Alejandro S, Cailliatte R, Alcon C, Dirick L, Domergue F, Correia D, Castaings L, Briat JF,
720 Mari S, Curie C. 2017. Intracellular Distribution of Manganese by the Trans-Golgi Network
721 Transporter NRAMP2 Is Critical for Photosynthesis and Cellular Redox Homeostasis. *Plant*
722 *Cell* 29:3068–3084.

723 Alejandro S, Höller S, Meier B, Peiter E. 2020. Manganese in Plants: From Acquisition to
724 Subcellular Allocation. *Front. Plant Sci.* 11:300.

725 Blaudez D, Kohler A, Martin F, Sanders D, Chalot M. 2003. Poplar metal tolerance protein 1
726 confers zinc tolerance and is an oligomeric vacuolar zinc transporter with an essential leucine
727 zipper motif. *Plant Cell* 15:2911–2928.

728 Cailliatte R, Schikora A, Briat JF, Mari S, Curie C. 2010. High-affinity manganese uptake by
729 the metal transporter NRAMP1 is essential for Arabidopsis growth in low manganese
730 conditions. *Plant Cell* 22:904–917.

731 Castaings L, Caquot A, Loubet S, Curie C. 2016. The high-affinity metal Transporters
732 NRAMP1 and IRT1 Team up to Take up Iron under Sufficient Metal Provision. *Sci. Rep.*
733 6:37222.

734 Chen J, Huang Y, Brachi B, Yun Q, Zhang W, Lu W, Li H, Li W, Sun X, Wang G, et al.
735 2019. Genome-wide analysis of Cushion willow provides insights into alpine plant divergence
736 in a biodiversity hotspot. *Nat. Commun.* 10:5230.

737 Cohen A, Nelson H, Nelson N. 2000. The family of SMF metal ion transporters in yeast cells.
738 *J. Biol. Chem.* 275:33388–33394.

739 Conant GC, Wolfe KH. 2008. Turning a hobby into a job: how duplicated genes find new
740 functions. *Nat. Rev. Genet.* 9:938–950.

741 Connorton JM, Balk J, Rodríguez-Celma J. 2017. Iron homeostasis in plants – a brief
742 overview. *Metallomics* 9:813–823.

743 Craciun AR, Meyer C-L, Chen J, Roosens N, De Groodt R, Hilson P, Verbruggen N. 2012.
744 Variation in HMA4 gene copy number and expression among Noccaea caerulescens
745 populations presenting different levels of Cd tolerance and accumulation. *J. Exp. Bot.*
746 63:4179–4189.

747 Curtis MD, Grossniklaus U. 2003. A Gateway Cloning Vector Set for High-Throughput
748 Functional Analysis of Genes in Planta. *Plant Physiol.* 133:462–469.

749 Dai X, Hu Q, Cai Q, Feng K, Ye N, Tuskan GA, Milne R, Chen Y, Wan Z, Wang Z, et al.
750 2014. The willow genome and divergent evolution from poplar after the common genome
751 duplication. *Cell Res.* 24:1274–1277.

752 Delhaize E, Gruber BD, Pittman JK, White RG, Leung H, Miao Y, Jiang L, Ryan PR,
753 Richardson AE. 2007. A role for the AtMTP11 gene of Arabidopsis in manganese transport

754 and tolerance. *Plant J* 51:198–210.

755 Ebine K, Fujimoto M, Okatani Y, Nishiyama T, Goh T, Ito E, Dainobu T, Nishitani A,
756 Uemura T, Sato MH, et al. 2011. A membrane trafficking pathway regulated by the plant-
757 specific RAB GTPase ARA6. *Nat. Cell Biol.* 13:853–859.

758 Eide D, Broderius M, Fett J, Guerinot ML. 1996. A novel iron-regulated metal transporter
759 from plants identified by functional expression in yeast. *Proc. Natl. Acad. Sci.* 93:5624–5628.

760 Eisenhut M, Hoecker N, Schmidt SB, Basgaran RM, Flachbart S, Jahns P, Eser T, Geimer S,
761 Husted S, Weber APM, et al. 2018. The Plastid Envelope CHLOROPLAST MANGANESE
762 TRANSPORTER1 Is Essential for Manganese Homeostasis in Arabidopsis. *Mol Plant*
763 11:955–969.

764 Eroglu S, Meier B, von Wiren N, Peiter E. 2016. The Vacuolar Manganese Transporter MTP8
765 Determines Tolerance to Iron Deficiency-Induced Chlorosis in Arabidopsis. *Plant Physiol*
766 170:1030–1045.

767 Flagel LE, Wendel JF. 2009. Gene duplication and evolutionary novelty in plants. *New*
768 *Phytol.* 183:557–564.

769 Freeling M. 2009. Bias in Plant Gene Content Following Different Sorts of Duplication:
770 Tandem, Whole-Genome, Segmental, or by Transposition. *Annu. Rev. Plant Biol.* 60:433–
771 453.

772 Gao H, Xie W, Yang C, Xu J, Li J, Wang H, Chen X, Huang CF. 2018. NRAMP2, a trans-
773 Golgi network-localized manganese transporter, is required for Arabidopsis root growth under
774 manganese deficiency. *New Phytol* 217:179–193.

775 Gao Y, Yang F, Liu J, Xie W, Zhang L, Chen Z, Peng Z, Ou Y, Yao Y. 2020. Genome-Wide
776 Identification of Metal Tolerance Protein Genes in Populus trichocarpa and Their Roles in
777 Response to Various Heavy Metal Stresses. *Int. J. Mol. Sci.* 21:1680.

778 Goodstein DM, Shu S, Howson R, Neupane R, Hayes RD, Fazo J, Mitros T, Dirks W,
779 Hellsten U, Putnam N, et al. 2012. Phytozome: a comparative platform for green plant
780 genomics. *Nucleic Acids Res.* 40:D1178–D1186.

781 Grefen C, Donald N, Hashimoto K, Kudla J, Schumacher K, Blatt MR. 2010. A ubiquitin-10
782 promoter-based vector set for fluorescent protein tagging facilitates temporal stability and
783 native protein distribution in transient and stable expression studies: Fluorescence tagging and
784 expression in Arabidopsis. *Plant J.* 64:355–365.

785 Hanikenne M, Kroymann J, Trampczynska A, Bernal M, Motte P, Clemens S, Krämer U.
786 2013. Hard selective sweep and ectopic gene conversion in a gene cluster affording
787 environmental adaptation. *PLoS Genet.* 9:e1003707.

788 He J, Li H, Ma C, Zhang Y, Polle A, Rennenberg H, Cheng X, Luo Z-B. 2015.
789 Overexpression of bacterial γ-glutamylcysteine synthetase mediates changes in cadmium
790 influx, allocation and detoxification in poplar. *New Phytol.* 205:240–254.

791 Hou J, Ye N, Dong Z, Lu M, Li L, Yin T. 2016. Major Chromosomal Rearrangements
792 Distinguish Willow and Poplar After the Ancestral "Salicoid" Genome Duplication. *Genome*
793 *Biol. Evol.* 8:1868–1875.

794 Inada N, Betsuyaku S, Shimada TL, Ebine K, Ito E, Kutsuna N, Hasezawa S, Takano Y,
795 Fukuda H, Nakano A, et al. 2016. Modulation of Plant RAB GTPase-Mediated Membrane
796 Trafficking Pathway at the Interface Between Plants and Obligate Biotrophic Pathogens.
797 *Plant Cell Physiol.* 57:1854–1864.

798 Jones DT, Taylor WR, Thornton JM. 1992. The rapid generation of mutation data matrices
799 from protein sequences. *Bioinformatics* 8:275–282.

800 Karimi M, Inzé D, Depicker A. 2002. GATEWAY™ vectors for Agrobacterium-mediated
801 plant transformation. *Trends Plant Sci.* 7:193–195.

802 Kramer U. 2005a. Phytoremediation: novel approaches to cleaning up polluted soils. *Curr*
803 *Opin Biotechnol* 16:133–141.

804 Kramer U. 2005b. MTP1 mops up excess zinc in Arabidopsis cells. *Trends Plant Sci.* 10:313–
805 315.

806 Krumsiek J, Arnold R, Rattei T. 2007. Gepard: a rapid and sensitive tool for creating dotplots
807 on genome scale. *Bioinformatics* 23:1026–1028.

808 Kumar S, Stecher G, Tamura K. 2016. MEGA7: Molecular Evolutionary Genetics Analysis
809 Version 7.0 for Bigger Datasets. *Mol. Biol. Evol.* 33:1870–1874.

810 Lamesch P, Berardini TZ, Li D, Swarbreck D, Wilks C, Sasidharan R, Muller R, Dreher K,
811 Alexander DL, Garcia-Hernandez M, et al. 2012. The Arabidopsis Information Resource
812 (TAIR): improved gene annotation and new tools. *Nucleic Acids Res.* 40:D1202–D1210.

813 Lanquar V, Lelièvre F, Bolte S, Hames C, Alcon C, Neumann D, Vansuyt G, Curie C,
814 Schroder A, Kramer U, et al. 2005. Mobilization of vacuolar iron by AtNRAMP3 and
815 AtNRAMP4 is essential for seed germination on low iron. *EMBO J* 24:4041–4051.

816 Lanquar V, Ramos MS, Lelievre F, Barbier-Brygoo H, Krieger-Liszkay A, Kramer U,
817 Thomine S. 2010. Export of vacuolar manganese by AtNRAMP3 and AtNRAMP4 is required
818 for optimal photosynthesis and growth under manganese deficiency. *Plant Physiol* 152:1986–
819 1999.

820 Le SQ, Gascuel O. 2008. An Improved General Amino Acid Replacement Matrix. *Mol. Biol.*
821 *Evol.* 25:1307–1320.

822 Leplé J-C, Brasileiro A-C, Michel M-F, Delmotte F., Jouanin L. 1992. Transgenic poplars:
823 expression of chimeric genes using four different constructs. *Plant Cell Rep.* [Internet] 11.
824 Available from: http://link.springer.com/10.1007/BF00232166

825 Li D, Xu X, Hu X, Liu Q, Wang Z, Zhang H, Wang Han, Wei M, Wang Hanzeng, Liu H, et
826 al. 2015. Genome-Wide Analysis and Heavy Metal-Induced Expression Profiling of the HMA
827 Gene Family in Populus trichocarpa. *Front. Plant Sci.* 6:1149.

828 Lin Y-C, Wang J, Delhomme N, Schiffthaler B, Sundström G, Zuccolo A, Nystedt B,
829 Hvidsten TR, de la Torre A, Cossu RM, et al. 2018. Functional and evolutionary genomic
830 inferences in *Populus* through genome and population sequencing of American and European
831 aspen. *Proc. Natl. Acad. Sci.* 115:E10970–E10978.

832 Luk EE, Culotta VC. 2001. Manganese superoxide dismutase in Saccharomyces cerevisiae

acquires its metal co-factor through a pathway involving the Nramp metal transporter, Smf2p. *J. Biol. Chem.* 276:47556–47562.

Migeon A, Blaudez D, Wilkins O, Montanini B, Campbell MM, Richaud P, Thomine S, Chalot M. 2010. Genome-wide analysis of plant metal transporters, with an emphasis on poplar. *Cell. Mol. Life Sci. CMLS* 67:3763–3784.

Ming R, Hou S, Feng Y, Yu Q, Dionne-Laporte A, Saw JH, Senin P, Wang W, Ly BV, Lewis KLT, et al. 2008. The draft genome of the transgenic tropical fruit tree papaya (Carica papaya Linnaeus). *Nature* 452:991–996.

Moriyama Y, Ito F, Takeda H, Yano T, Okabe M, Kuraku S, Keeley FW, Koshiba-Takeuchi K. 2016. Evolution of the fish heart by sub/neofunctionalization of an elastin gene. *Nat. Commun.* 7:10397.

Müdsam C, Wollschläger P, Sauer N, Schneider S. 2018. Sorting of *Arabidopsis* NRAMP3 and NRAMP4 depends on adaptor protein complex AP4 and a dileucine-based motif. *Traffic* 19:503–521.

Nei, M, Gojobori, T. 1986. Simple methods for estimating the numbers of synonymous and nonsynonymous nucleotide substitutions. *Mol. Biol. Evol.* [Internet]. Available from: https://academic.oup.com/mbe/article/3/5/418/988012/Simple-methods-for-estimating-the-numbers-of

Ó Lochlainn S, Bowen HC, Fray RG, Hammond JP, King GJ, White PJ, Graham NS, Broadley MR. 2011. Tandem Quadruplication of HMA4 in the Zinc (Zn) and Cadmium (Cd) Hyperaccumulator Noccaea caerulescens.Baxter I, editor. *PLoS ONE* 6:e17814.

One Thousand Plant Transcriptomes Initiative. 2019. One thousand plant transcriptomes and the phylogenomics of green plants. *Nature* 574:679–685.

Oomen RJFJ, Wu J, Lelièvre F, Blanchet S, Richaud P, Barbier-Brygoo H, Aarts MGM, Thomine S. 2009. Functional characterization of NRAMP3 and NRAMP4 from the metal hyperaccumulator *Thlaspi caerulescens*. *New Phytol.* 181:637–650.

Peiter E, Montanini B, Gobert A, Pedas P, Husted S, Maathuis FJ, Blaudez D, Chalot M, Sanders D. 2007. A secretory pathway-localized cation diffusion facilitator confers plant manganese tolerance. *Proc Natl Acad Sci U A* 104:8532–8537.

Portnoy ME, Liu XF, Culotta VC. 2000. Saccharomyces cerevisiae expresses three functionally distinct homologues of the Nramp family of metal transporters. *Mol. Cell. Biol.* 20:7893–7902.

Pottier M., Garcia de la Torre VS, Victor C, David LC, Chalot M, Thomine S. 2015a. Genotypic variations in the dynamics of metal concentrations in poplar leaves: a field study with a perspective on phytoremediation. *Env. Pollut* 199:73–82.

Pottier M., Oomen R., Picco C., Giraudat J., Scholz-Starke J., Richaud P., Carpaneto A., Thomine S. 2015b. Identification of mutations allowing Natural Resistance Associated Macrophage Proteins (NRAMP) to discriminate against cadmium. *Plant J.* 83:625–637.

Proost S, Pattyn P, Gerats T, Van de Peer Y. 2011. Journey through the past: 150 million years of plant genome evolution: One hundred and fifty million years of plant genome

873 evolution. *Plant J.* 66:58–65.

874 Ravet K, Danford FL, Dihle A, Pittarello M, Pilon M. 2011. Spatiotemporal analysis of
875 copper homeostasis in Populus trichocarpa reveals an integrated molecular remodeling for a
876 preferential allocation of copper to plastocyanin in the chloroplasts of developing leaves.
877 *Plant Physiol.* 157:1300–1312.

878 Ren L-L, Liu Y-J, Liu H-J, Qian T-T, Qi L-W, Wang X-R, Zeng Q-Y. 2014. Subcellular
879 Relocalization and Positive Selection Play Key Roles in the Retention of Duplicate Genes of
880 *Populus* Class III Peroxidase Family. *Plant Cell* 26:2404–2419.

881 Rentsch D, Laloi M, Rouhara I, Schmelzer E, Delrot S, Frommer WB. 1995. *NTR1* encodes a
882 high affinity oligopeptide transporter in *Arabidopsis*. *FEBS Lett.* 370:264–268.

883 Sayers EW, Beck J, Bolton EE, Bourexis D, Brister JR, Canese K, Comeau DC, Funk K, Kim
884 S, Klimke W, et al. 2021. Database resources of the National Center for Biotechnology
885 Information. *Nucleic Acids Res.* 49:D10–D17.

886 Schneider A, Steinberger I, Herdean A, Gandini C, Eisenhut M, Kurz S, Morper A, Hoecker
887 N, Ruhle T, Labs M, et al. 2016. The Evolutionarily Conserved Protein PHOTOSYNTHESIS
888 AFFECTED MUTANT71 Is Required for Efficient Manganese Uptake at the Thylakoid
889 Membrane in Arabidopsis. *Plant Cell* 28:892–910.

890 Schneider CA, Rasband WS, Eliceiri KW. 2012. NIH Image to ImageJ: 25 years of image
891 analysis. *Nat. Methods* 9:671–675.

892 Seregin IV, Kozhevnikova AD. 2020. Low-molecular-weight ligands in plants: role in metal
893 homeostasis and hyperaccumulation. *Photosynth. Res.*

894 Shen JR. 2015. The Structure of Photosystem II and the Mechanism of Water Oxidation in
895 Photosynthesis. *Annu Rev Plant Biol* 66:23–48.

896 Sjödin A, Street NR, Sandberg G, Gustafsson P, Jansson S. 2009. The *Populus* Genome
897 Integrative Explorer (PopGenIE): a new resource for exploring the *Populus* genome. *New*
898 *Phytol.* 182:1013–1025.

899 Steinway SN, Dannenfelser R, Laucius CD, Hayes JE, Nayak S. 2010. JCoDA: a tool for
900 detecting evolutionary selection. *BMC Bioinformatics* 11:284.

901 Supek F, Supekova L, Nelson H, Nelson N. 1996. A yeast manganese transporter related to
902 the macrophage protein involved in conferring resistance to mycobacteria. *Proc. Natl. Acad.*
903 *Sci.* 93:5105–5110.

904 Thomine S, Lelièvre F, Debarbieux E, Schroeder JI, Barbier-Brygoo H. 2003. AtNRAMP3, a
905 multispecific vacuolar metal transporter involved in plant responses to iron deficiency:
906 *NRAMP vacuolar metal transporter*. *Plant J.* 34:685–695.

907 Thomine S, Wang R, Ward JM, Crawford NM, Schroeder JI. 2000. Cadmium and iron
908 transport by members of a plant transporter gene family in *Arabidopsis* with homology to
909 *NRAMP* genes. *Proc Nat Acad Sci USA* 97:4991–4996.

910 Tuskan GA, DiFazio S, Jansson S, Bohlmann J, Grigoriev I, Hellsten U, Putnam N, Ralph S,
911 Rombauts S, Salamov A, et al. 2006. The Genome of Black Cottonwood, Populus trichocarpa

(Torr. & Gray). *Science* 313:1596–1604.

Tuskan GA, et al. 2006. The genome of black cottonwood, Populus trichocarpa (Torr. & Gray). *Science* 313:1596–1604.

Uemura T, Kim H, Saito C, Ebine K, Ueda T, Schulze-Lefert P, Nakano A. 2012. Qa-SNAREs localized to the trans-Golgi network regulate multiple transport pathways and extracellular disease resistance in plants. *Proc. Natl. Acad. Sci.* 109:1784–1789.

Uemura T, Nakano RT, Takagi J, Wang Y, Kramer K, Finkemeier I, Nakagami H, Tsuda K, Ueda T, Schulze-Lefert P, et al. 2019. A Golgi-Released Subpopulation of the Trans-Golgi Network Mediates Protein Secretion in Arabidopsis. *Plant Physiol.* 179:519–532.

Vidal SM, Malo D, Vogan K, Skamene E, Gros P. 1993. Natural Resistance to Infection With Intracellular Parasites - Isolation of a Candidate For Bcg. *Cell* 73:469–485.

Viotti C, Bubeck J, Stierhof Y-D, Krebs M, Langhans M, van den Berg W, van Dongen W, Richter S, Geldner N, Takano J, et al. 2010. Endocytic and Secretory Traffic in *Arabidopsis* Merge in the Trans-Golgi Network/Early Endosome, an Independent and Highly Dynamic Organelle. *Plant Cell* 22:1344–1357.

Wang H, Liu Yuanyuan, Peng Z, Li J, Huang W, Liu Yan, Wang X, Xie S, Sun L, Han E, et al. 2019. Ectopic Expression of Poplar ABC Transporter PtoABCG36 Confers Cd Tolerance in Arabidopsis thaliana. *Int. J. Mol. Sci.* 20.

Wang M, Zhang L, Zhang Z, Li M, Wang D, Zhang X, Xi Z, Keefover‐Ring K, Smart LB, DiFazio SP, et al. 2020. Phylogenomics of the genus *Populus* reveals extensive interspecific gene flow and balancing selection. *New Phytol.* 225:1370–1382.

Wessling-Resnick M. 2015. Nramp1 and Other Transporters Involved in Metal Withholding during Infection. *J. Biol. Chem.* 290:18984–18990.

Whelan S, Goldman N. 2001. A General Empirical Model of Protein Evolution Derived from Multiple Protein Families Using a Maximum-Likelihood Approach. *Mol. Biol. Evol.* 18:691–699.

White SE, Habera LF, Wessler SR. 1994. Retrotransposons in the flanking regions of normal plant genes: a role for copia-like elements in the evolution of gene structure and expression. *Proc. Natl. Acad. Sci.* 91:11792–11796.

Yang Chang-Hong, Wang C, Singh S, Fan N, Liu S, Zhao L, Cao H, Xie W, Yang Chengwei, Huang C. 2021. Golgi-localised manganese transporter PML3 regulates *Arabidopsis* growth through modulating Golgi glycosylation and cell wall biosynthesis. *New Phytol.*:nph.17209.

Yang X, Tuskan GA, Cheng (Max) Zong-Ming. 2006. Divergence of the Dof Gene Families in Poplar, Arabidopsis, and Rice Suggests Multiple Modes of Gene Evolution after Duplication. *Plant Physiol.* 142:820–830.

Zhang B, Zhang C, Liu C, Jing Y, Wang Y, Jin L, Yang L, Fu A, Shi J, Zhao F, et al. 2018. Inner Envelope CHLOROPLAST MANGANESE TRANSPORTER 1 Supports Manganese Homeostasis and Phototrophic Growth in Arabidopsis. *Mol Plant* 11:943–954.

Zhang B, Zhu W, Diao S, Wu X, Lu J, Ding C, Su X. 2019. The poplar pangenome provides

951 insights into the evolutionary history of the genus. *Commun. Biol.* 2:215.

952 Zhang J. 2003. Evolution by gene duplication: an update. *Trends Ecol. Evol.* 18:292–298.

953 Zhou R, Macaya-Sanz D, Rodgers-Melnick E, Carlson CH, Gouker FE, Evans LM, Schmutz
954 J, Jenkins JW, Yan J, Tuskan GA, et al. 2018. Characterization of a large sex determination
955 region in Salix purpurea L. (Salicaceae). *Mol. Genet. Genomics* 293:1437–1452.

956

957

958

959

960

961 Figure legends

962 **Fig. 1.** Collinearity between *Salix purpurea* and *Populus trichocarpa* genomes in the area
963 surrounding *NRAMP3* loci. Gene collinearity between *P. trichocarpa* and *S. purpurea* is
964 maintained around *NRAMP3* loci. (A) Dot-plots performed on Gepard software V1.40
965 (Krumsiek *et al*., 2007), using 107 kb and 140 kb sequences of *S. purpurea* and *P. trichocarpa*
966 genomes centered on *NRAMP3* loci, respectively. Sequence homology between *S. purpurea*
967 and *P. trichocarpa* are indicated by black dots. Red arrows indicate homology between
968 *SapurNRAMP3* and *PotriNRAMP3.2* as well as between *SapurNRAMP3* and *PotriNRAMP3.1*.
969 (B) Schematic representation of the genomic sequence around *NRAMP3* locus in *P. trichocarpa*
970 and *S. purpurea*.

971

972 **Fig. 2.** Phylogenetic tree of NRAMP3 homologues in *Populus* and *Salix* species. *Arabidopsis*
973 *thaliana* NRAMP2, NRAMP3 and NRAMP4 as well as NRAMP2 genes from *Populus*
974 *trichocarpa* and *Salix purpurea* are shown as an outgroup. $^{\$}$ indicates incomplete protein
975 sequences. Phylogenetic analyses were conducted as described in Materials and Methods.
976 Protein sequences used for this tree are listed in supplementary data S3.

977

978 **Fig. 3.** Alignment of the consensus sequences of *Populus* NRAMP3.1 and NRAMP3.2. The
979 consensus sequences were determined from the NRAMP alignments shown in supplementary
980 figure S3. Asterisk indicates less than 90% of conservation within *Populus* NRAMP3.1 or
981 NRAMP3.2 cluster. Identical, similar and different residues between the two consensus
982 sequences are indicated in black, blue, and red, respectively. Frames indicate residues under
983 purifying selection and green arrows indicate positive selection in either *Populus NRAMP3.1*
984 or *NRAMP3.2* cluster according to the FEL method ($p < 0.05$). Note that NRAMP3.1 sequences
985 contain an insertion of one residue at position 4 leading to a gap (-) in NRAMP3.2 sequences.

986

987 **Fig. 4.** *PotriNRAMP3.1* and *PotriNRAMP3.2* encode functional Mn transporters. Functional
988 complementation of *smf1* (A) and *smf2* (B) yeast mutants. Yeast cells were transformed with
989 pDR195gtw vector containing the cDNA of *GUS, AtNRAMP1 AtNRAMP2*, *PotriNRAMP3.1* or
990 *PotriNRAMP3.2*. Transformed yeasts were grown overnight in liquid synthetic dextrose -ura.

The cultures were diluted to ODs of 1 to 10^{-3} and spotted on synthetic dextrose -ura plates. Transformed *smf1* (A) strains were grown on medium supplemented with 5 mM EGTA and 100 µM $MnSO_4$ (+ Mn) or with 5 mM EGTA without $MnSO_4$ (- Mn). Transformed *smf2* (B) strains were grown in medium supplemented with 10 mM EGTA and 100 µM $MnSO_4$ (+ Mn), with 5 mM EGTA without MnSO4 (- Mn) or with 10 mM $MnSO_4$ (+++ Mn). The plates were incubated at 30°C for 5 days (*smf1*) or 2 days (*smf2*) before photography. White lines indicate cropping, unmodified pictures are shown as supplementary figures S4 and S5. (C) Expression of *PotriNRAMP3.1* or *PotriNRAMP3.2* increases Mn accumulation in yeast cells. Liquid SD -ura medium containing *smf2* cells expressing *GUS*, *AtNRAMP4*, *PotriNRAMP3.1* or *PotriNRAMP3.2* were grown overnight and diluted to OD 0.3 in liquid SD -ura supplemented with 30 µM $FeCl_3$ and 10 µM $MnSO_4$. After 30 hrs of incubation at 30°C, yeast cells were washed twice, and metal concentrations were determined by atomic absorption spectrometry. Error bars represent the SD. Asterisks indicate significant differences with control cells expressing *GUS* according to a Mann–Whitney test ($p < 0.05$).

Fig. 5. PotriNRAMP3.1 and PotriNRAMP3.2 transport Fe. Functional complementation of the *fet3fet4* yeast iron uptake mutant by *PotriNRAMP3.1* and *PotriNRAMP3.2*. *fet3fet4* yeast cells were transformed with pDR195gtw vector containing the cDNA of *GUS*, *AtNRAMP1*, *AtNRAMP4*, *PotriNRAMP3.1* and *PotriNRAMP3.2*. Transformed *fet3fet4* yeasts were grown overnight in liquid synthetic dextrose -ura supplemented with 0.2 mM $FeCl_3$. Cultures were diluted to ODs of 1 to 10^{-3} and spotted on synthetic dextrose -ura plates supplemented with 100 µM of the Fe chelator BathoPhenanthroline-Di-Sulfonic acid (BPDS) and 0.2 mM $FeCl_3$ (+ Fe) or with 100 µM BPDS and 40 µM $FeCl_3$ (- Fe). The plates were incubated at 30°C for 4 days before photography.

Fig. 6. *PotriNRAMP3.1* and *PotriNRAMP3.2* are both expressed in all organs. *PotriNRAMP3.1* and *PotriNRAMP3.2* transcript levels were determined by RT-qPCR using specific primers for each isoform and normalization by three reference genes, *i.e.*, *UBIQ*, *EF1* and *PP2A*. The graph shows means ± SD of three replicates on different individuals.

Fig. 7. *PotriNRAMP3.2* but not *PotriNRAMP3.1* expression complements the Arabidopsis *nramp3nramp4* double mutant growth defects under iron starvation. (A) Representative pictures of *nramp3nramp4 pUb10:PotriNRAMP3.1 and pUb10:PotriNRAMP3.2 T3* Arabidopsis lines together with wild-type (Col-0) as positive control and *nramp3nramp4* as negative control grown vertically in ABIS supplemented with 50 µM FeHBED for 8 days (control, bottom panel) or without iron for 8 days (- Fe, top panel). (B) Quantification of main root lengths of wild-type (Col-0), *nramp3nramp4* and 3 independent *nramp3nramp4 pUb10:PotriNRAMP3.1 and pUb10:PotriNRAMP3.2 T3* lines. Values represent mean of 10–12 roots and bars represent SD. Different letters reflect significant differences according to a Kruskal-Wallis test followed by Dunn's test for multiple comparison ($p < 0.01$). No significant differences among genotypes were detected in the presence of Fe (B).

Fig. 8. PotriNRAMP3.1 (A) and PotriNRAMP3.2 (B) localize to different cellular compartments in both Arabidopsis and Poplar. GFP translational fusions of PotriNRAMP3.1 (A) and PotriNRAMP3.2 (B) were imaged by spinning disk confocal microscopy in transgenic Arabidopsis (*Left*) and Poplar (*Right*). NRAMP3.1-GFP labels granular cytoplasmic structures at the cell periphery, in both Arabidopsis and Poplar. In contrast, NRAMP3.2-GFP is present on the vacuolar membrane. Images represent vacuolar planes of root epidermal cells (early elongation zone). Transmitted-light (differential interference contrast, *DIC*) and fluorescence (*GFP)* acquisitions are shown. Scale bar : 10 µm.

Fig. 9. PotriNRAMP3.1-GFP localizes to the TGN compartment. (A) Colocalisation of PotriNRAMP3.1-GFP with the Trans-Golgi Network (TGN) marker mRFP-SYP43. (B) Juxtaposition of PotriNRAMP3.1-GFP with the trans-Golgi apparatus marker mRFP-ST. Note how PotriNRAMP3.1-GFP signal either faces the center of the toroidal structure of the trans-Golgi or is present as Golgi-independent structures (white asterisks). On the merged images the overlap of GFP (green) and mRFP (magenta) channels appears white. Spinning disk confocal images were acquired in the cortical planes of root epidermal cells in the early elongation zone of Arabidopsis F1 seedlings. Scale bar : 10 µm. Super resolution acquisitions (*Super Res.*) are 10 µm wide.

Fig. 10. The ectopic over expression of *PotriNRAMP3.1* but not that of *PotriNRAMP3.2* leads to phenotypic alterations in poplar. Overview of transgenic poplar expressing *PotriNRAMP3.1-GFP* (A, purple tags) or *PotriNRAMP3.2-GFP* (B, orange tags) along with NT control (A and B, white tag), 2 months after transfer from *in vitro* to soil. (C) Mean heights of poplar from the different genotypes. Error bars represent SE (n = 4-7). Asterisks denote significant difference with respect to NT control according to a Mann-Whitney test (*: $p < 0.05$, **: $p < 0.01$). (D-I) Leaf phenotypes of representative trees. (D,E) NT control, (F,G) PotriNRAMP3.1-GFP line 9 (H,I) PotriNRAMP3.2-GFP, line 12. (D, F, H) pictures; (E, G, I) PS II maximum quantum yield measured with imaging Pulse-Amplitude-Modulation. Relative *PotriNRAMP3.1* and *PotriNRAMP3.2* mRNA levels of OE lines are shown in supplementary figure S11.

Fig. 11. Ectopic over expression of *PotriNRAMP3.1-GFP* but not that of *PotriNRAMP3.2-GFP* perturbs Mn distribution in poplar leaves. Mn concentrations in senescent (A), mature (B), young leaves (C) and young stems (D) of poplars 2 months after transfer from *in vitro* to soil was determined using Atomic Emission Spectroscopy. Mean Mn concentrations of PotriNRAMP3.1-GFP or PotriNRAMP3.2-GFP OE lines were compared with NT control. Error bars represent SD (n = 4-7). Asterisks denote significant differences with the NT control according to a Mann-Whitney test (*: $p < 0.05$, **: $p < 0.01$). (E) Mean Mn concentrations in veins and lamina of leaves from NT control and 4 *PotriNRAMP3.1-GFP* OE lines. Error bars represent SD (n = 3-6). Asterisks denote significant differences between veins and lamina according to a Mann-Whitney test (*: $p < 0.05$, **: $p < 0.01$). Different letters denote significant differences among genotypes in the lamina (lowercase) or in the veins (capitals) according to a Kruskal-Wallis test followed by Dunn's test for multiple comparison ($p < 0.01$).

Fig. 12. Working model to account of PotriNRAMP3.1 role in Mn transport from cell to cell. The model is based on the hypothesis that Mn moves through the transcellular pathway, being secreted in the apoplast via exocytosis by the cells proximal to the veins and taken up by the cells that are distal to the veins. According to this hypothesis, the transporters loading (PotriMTP11) or unloading (PotriNRAMP3.1 as well as PotriNRAMP2 assuming function conservation with Arabidopsis AtNRAMP2) Mn from the secretory pathway would determine the amount of Mn made available by proximal cells for uptake by distal cells. In this context,

1083 efficient removal of Mn from the secretory pathway in the proximal cells by PotriNRAMP3.1
1084 overexpression would limit Mn availability for the distal cell.

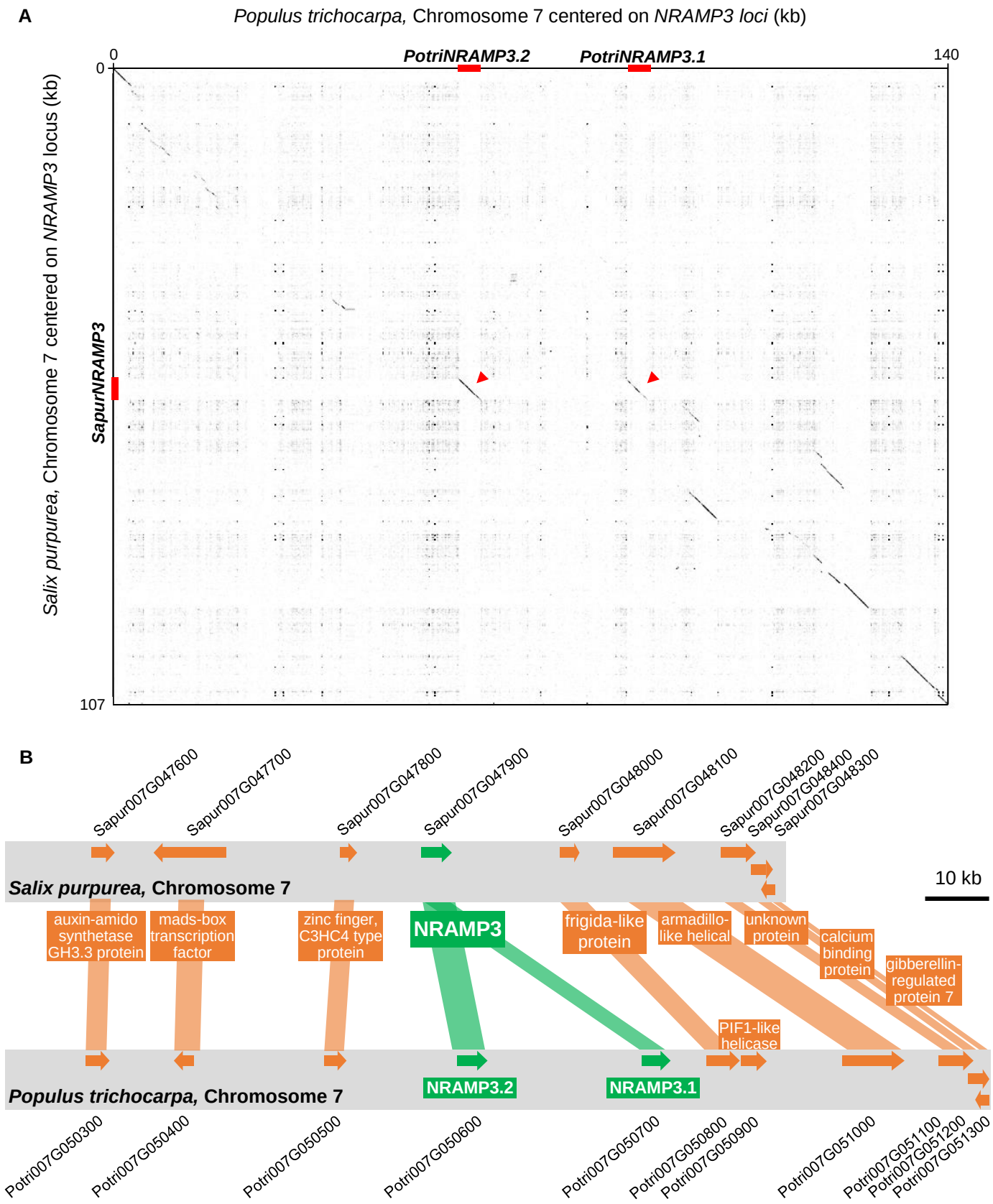

Fig. 1. Collinearity between *Salix purpurea* and *Populus trichocarpa* genomes in the area surrounding *NRAMP3* loci. Gene collinearity between *P. trichocarpa* and *S. purpurea* is maintained around *NRAMP3* loci. (A) Dot-plots centered on *NRAMP3* loci, performed on Gepard software V1.40 (Krumsiek *et al.,* 2007), using 107 kb and 140 kb sequences of *S. purpurea* and *P. trichocarpa* genomes, respectively. Sequence homology between *S. purpurea* and *P. trichocarpa* are indicated by black dots. Red arrows indicate homology between *SapurNRAMP3* and *PotriNRAMP3.2* as well as between *SapurNRAMP3* and *PotriNRAMP3.1.* (B) Schematic representation of the genomic sequence around *NRAMP3* loci in *P. trichocarpa* and *S. purpurea*.

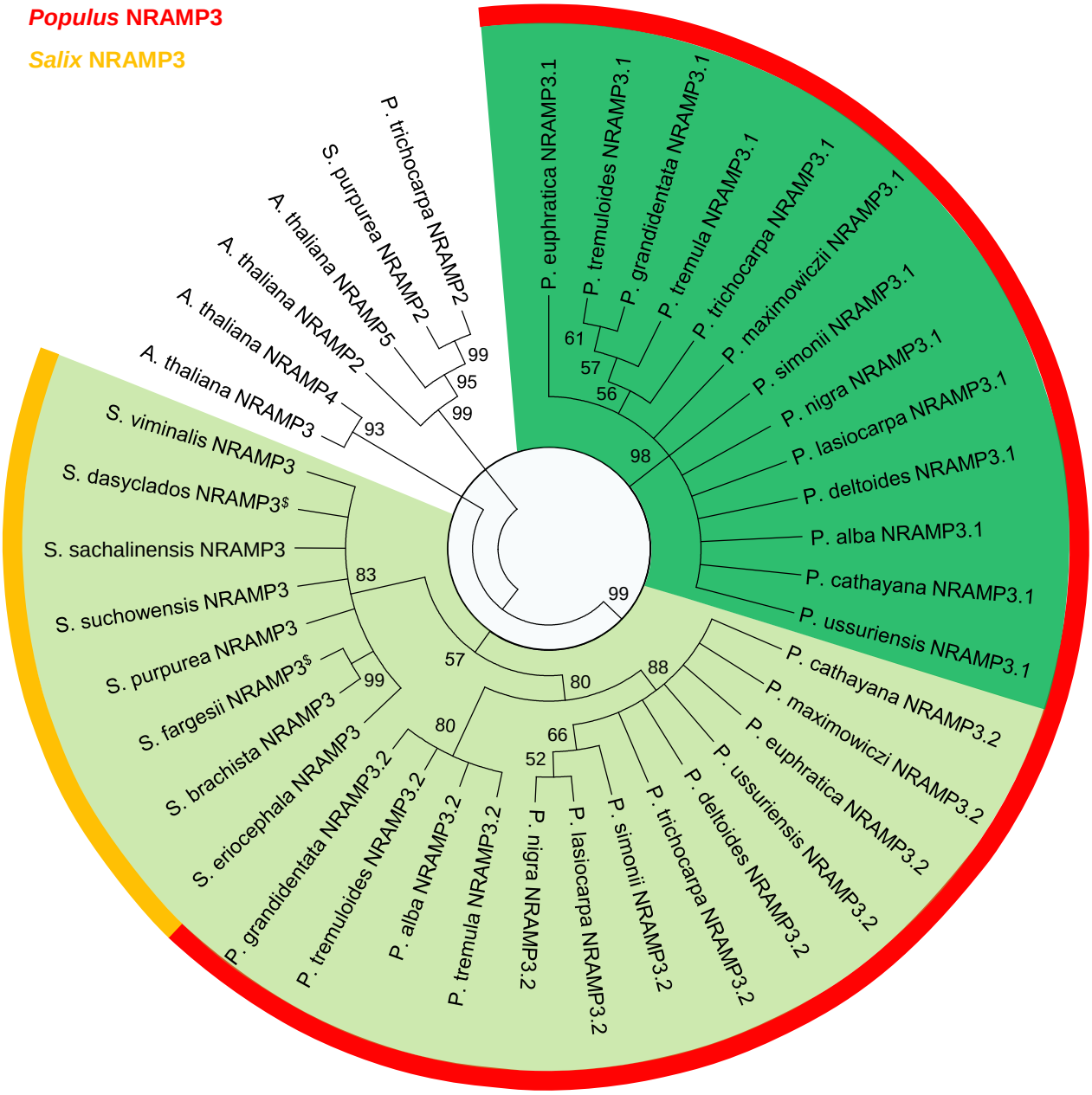

Fig. 2. Phylogenetic tree of NRAMP3 homologues in *Populus* and *Salix* species. *A. thaliana* NRAMP2, NRAMP3 and NRAMP4 as well as *P. trichocarpa* and *S. purpurea* NRAMP2 genes are shown as an outgroup. $ indicates incomplete protein sequences. Phylogenetic analyses were conducted as described in Materials and Methods. Protein sequences used for this tree are listed in supplementary data S3.

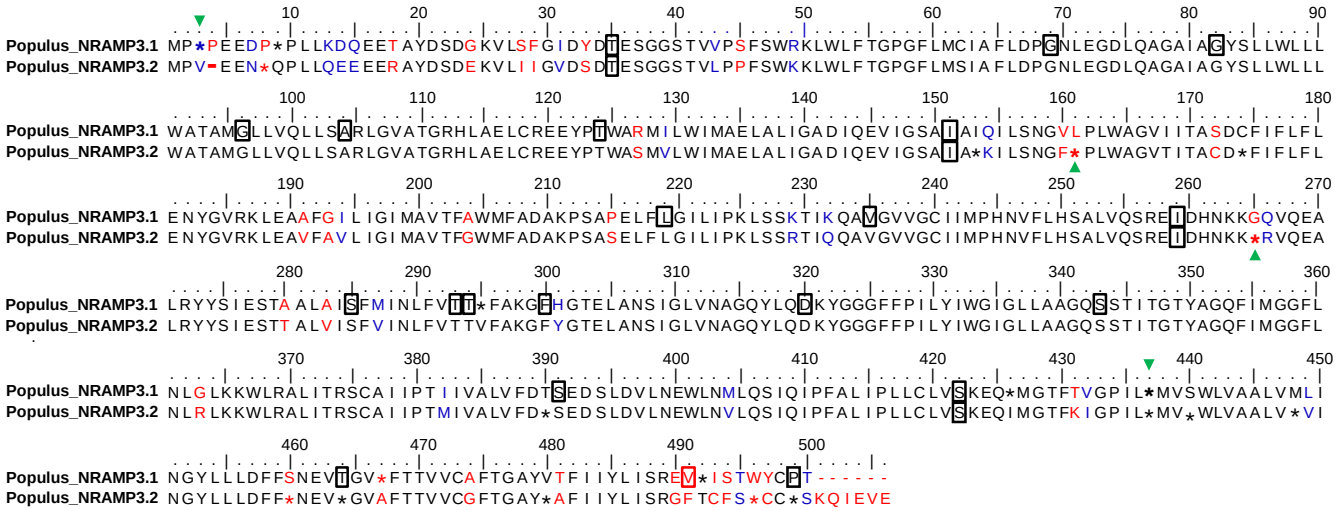

Fig. 3. Alignment of the consensus sequences of *Populus* NRAMP3.1 and NRAMP3.2. The consensus sequences were determined from the NRAMP alignments shown in supplementary figure S3. Asterisk indicates less than 90% of conservation within *Populus* NRAMP3.1 or NRAMP3.2 cluster. Identical, similar and different residues between the two consensus sequences are indicated in black, blue, and red, respectively. Frames indicate residues under purifying selection and green arrows indicate positive selections in either *Populus* NRAMP3.1 or NRAMP3.2 cluster according to the FEL method ($p < 0.05$). Note that NRAMP3.1 sequences contain an insertion of residue at position 4, leading to a gap (-) in NRAMP3.2 sequences.

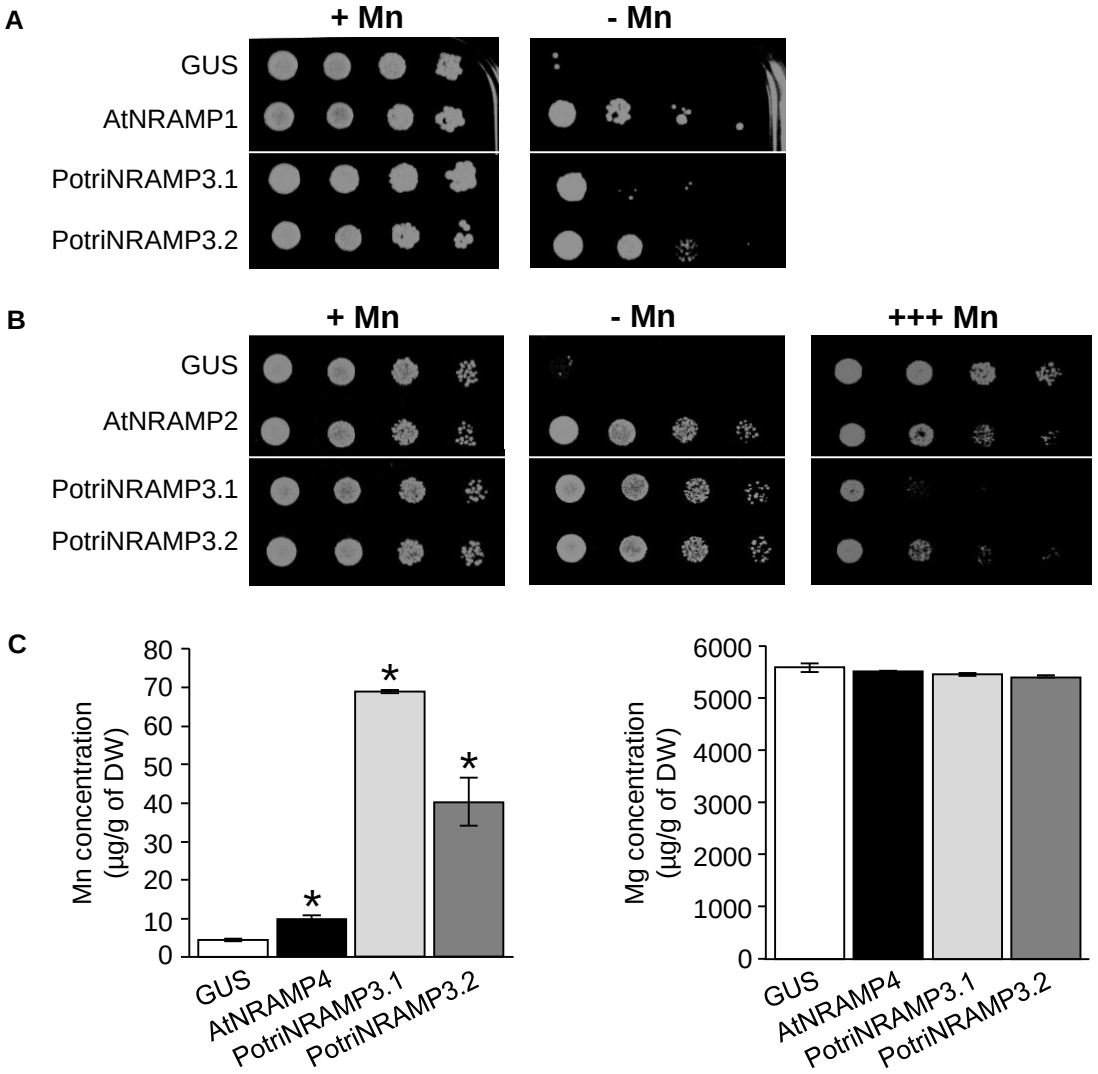

Fig. 4. *PotriNRAMP3.1* and *PotriNRAMP3.2* encode functional Mn transporters. Functional complementation of *smf1* (A) and *smf2* (B) yeast mutants. Yeast cells were transformed with pDR195gtw vector containing the cDNA of *GUS, AtNRAMP1 AtNRAMP2*, *PotriNRAMP3.1* or *PotriNRAMP3.2*. Transformed yeasts were grown overnight in liquid synthetic dextrose -ura. The cultures were diluted to ODs of 1 to 10^{-3} and spotted on synthetic dextrose -ura plates. Transformed *smf1* (A) strains were grown on medium supplemented with 5 mM EGTA and 100 µM $MnSO_4$ (+ Mn) or with 5 mM EGTA without $MnSO_4$ (- Mn). Transformed *smf2* (B) strains were grown in medium supplemented with 10 mM EGTA and 100 µM $MnSO_4$ (+ Mn), with 5 mM EGTA without MnSO4 (- Mn) or with 10 mM $MnSO_4$ (+++ Mn). The plates were incubated at 30°C for 5 days (*smf1*) or 2 days (*smf2*) before photography. White lines indicate cropping, unmodified pictures are shown as supplementary figures S4 and S5. (C) Expression of *PotriNRAMP3.1* or *PotriNRAMP3.2* increase Mn accumulation in yeast cells. Liquid SD -ura medium containing *smf2* cells expressing *GUS*, *AtNRAMP4*, *PotriNRAMP3.1* or *PotriNRAMP3.2* were grown overnight and diluted to OD 0.3 in liquid SD -ura supplemented with 30 µM $FeCl_3$ and 10 µM $MnSO_4$. After 30 hrs of incubation at 30°C, yeast cells were washed twice, and metal concentrations were determined by atomic absorption spectrometry. Error bars represent the SD. Asterisk indicate significant differences with control cells expressing *GUS* according to a Mann–Whitney test ($p < 0.05$).

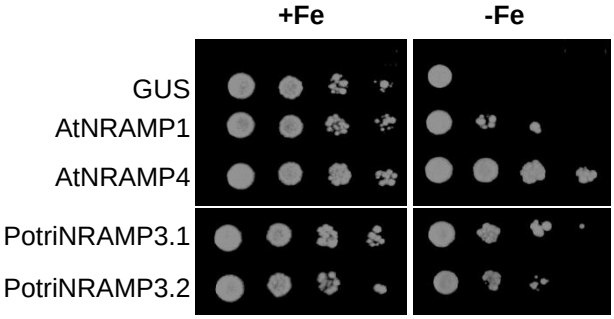

Fig. 5. PotriNRAMP3.1 and PotriNRAMP3.2 transport Fe. Functional complementation of the *fet3fet4* yeast iron uptake mutant by *PotriNRAMP3.1* and *PotriNRAMP3.2*. *fet3fet4* yeast cells were transformed with pDR195gtw vector containing the cDNA of *GUS, AtNRAMP1, AtNRAMP4*, *PotriNRAMP3.1* and *PotriNRAMP3.2*. Transformed *fet3fet4* yeasts were grown overnight in liquid synthetic dextrose -ura supplemented with 0.2 mM $FeCl_3$. Cultures were diluted to ODs of 1 to 10^{-3} and spotted on synthetic dextrose -ura plates supplemented with 100 µM of the Fe chelator BathoPhenanthroline-Di-Sulfonic acid (BPDS) and 0.2 mM $FeCl_3$ (+ Fe) or with 100 µM BPDS and 40 µM $FeCl_3$ (- Fe). The plates were incubated at 30°C for 4 days before photography.

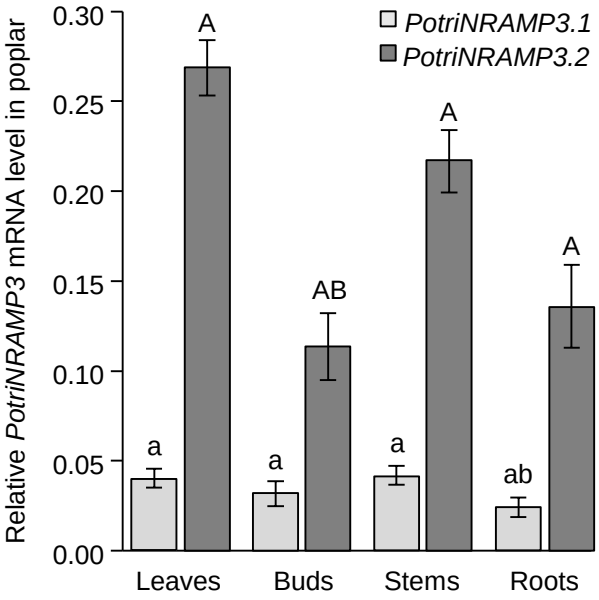

Fig. 6. *PotriNRAMP3.1* and *PotriNRAMP3.2* are both expressed in all organs. *PotriNRAMP3.1* and *PotriNRAMP3.2* transcript levels were determined by RT-qPCR using specific primers for each isoform and normalization by three reference genes, *i.e., UBQ*, *EF1,* and *PP2A*. The graph shows means ± SD of 4 replicates on different individuals. Different letters denote significant differences among organs for *PotriNRAMP3.1* (lowercase) or *PotriNRAMP3.2* (capitals) according to a Kruskal-Wallis test followed by Dunn's test for multiple comparison ($p < 0.01$).

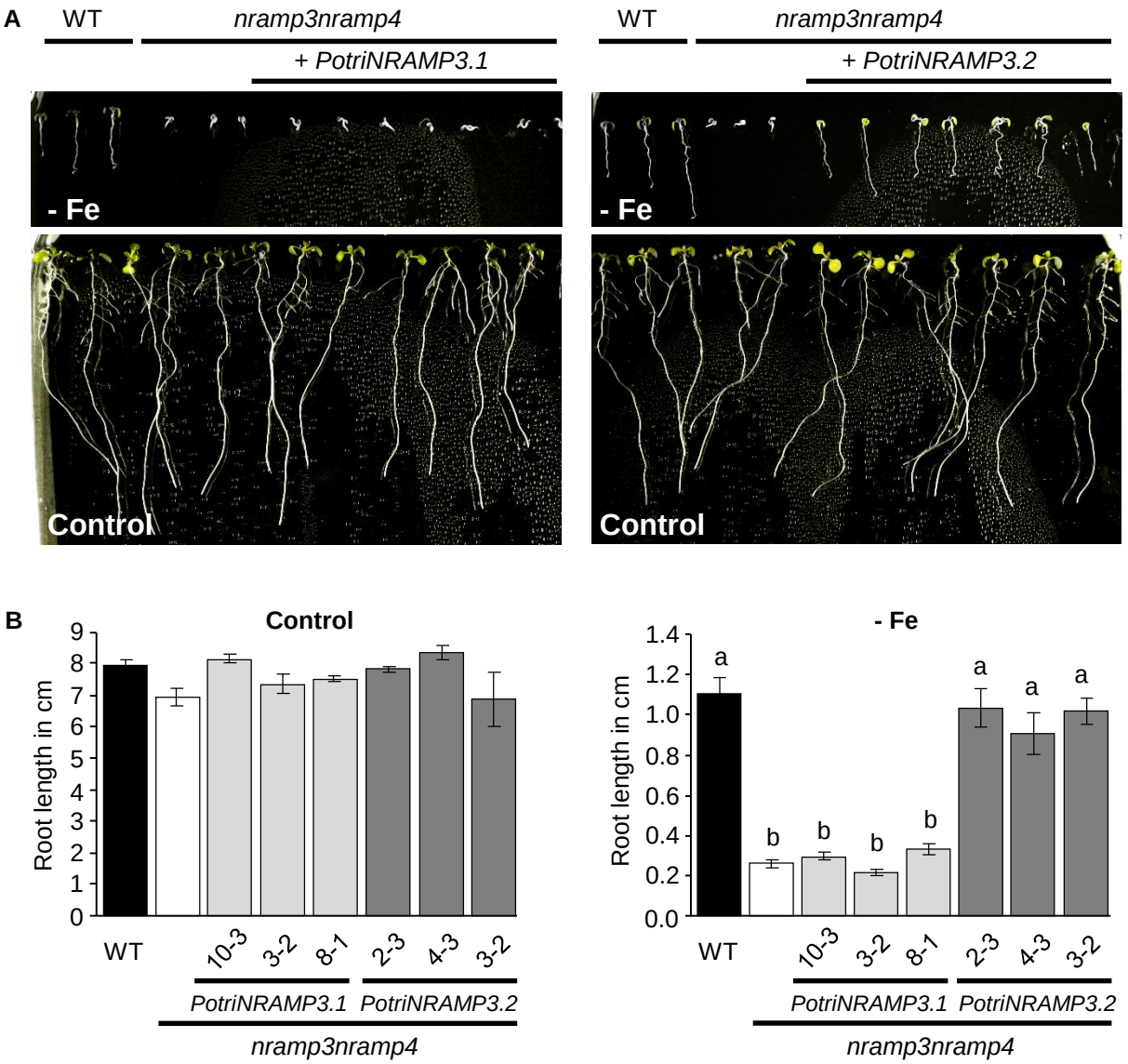

Fig. 7. *PotriNRAMP3.2* but not *PotriNRAMP3.1* expression complements the Arabidopsis *nramp3nramp4* double mutant growth defects under iron starvation. (A) Representative pictures of *nramp3nramp4 pUb10:PotriNRAMP3.1 and pUb10:PotriNRAMP3.2 T3* Arabidopsis lines together with wild-type (Col-0) as positive control and *nramp3nramp4* as negative control grown vertically for 8 days in ABIS supplemented with 50 µM FeHBED (control, bottom panel) or without iron (- Fe, top panel). (B) Quantification of main root lengths of wild-type (Col-0), *nramp3nramp4* and 3 independent *nramp3nramp4 pUb10:PotriNRAMP3.1 and pUb10:PotriNRAMP3.2 T3* lines. Values represent mean of 10–12 roots and bars represent SD. Different letters reflect significant differences according to a Kruskal-Wallis test followed by Dunn's test for multiple comparison ($p < 0.01$). No significant differences among genotypes were detected in the presence of Fe, left panel in (B).

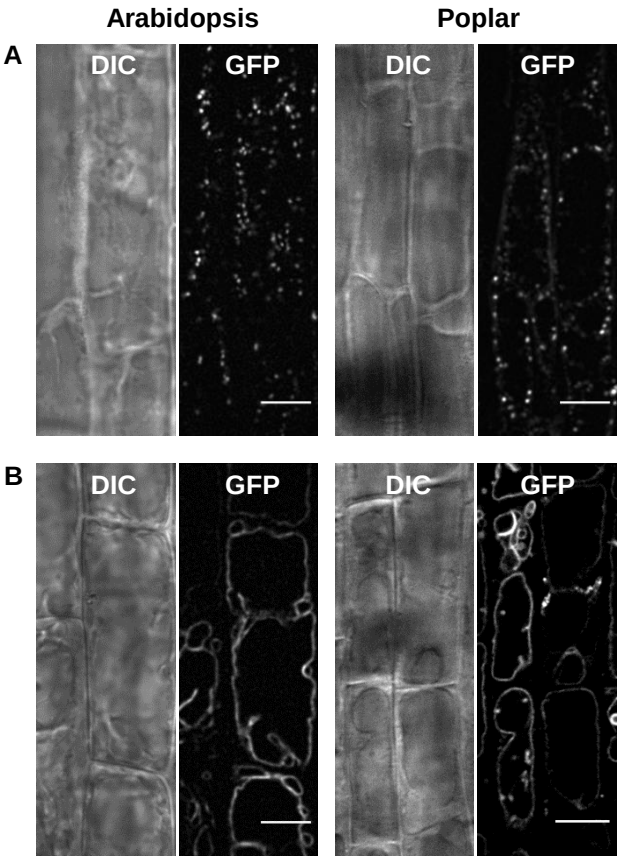

Fig. 8. PotriNRAMP3.1 (A) and PotriNRAMP3.2 (B) localize to different cellular compartments in both Arabidopsis and Poplar. GFP translational fusions of PotriNRAMP3.1 (A) and PotriNRAMP3.2 (B) were imaged by spinning disk confocal microscopy in transgenic Arabidopsis (*Left*) and Poplar (*Right*). NRAMP3.1-GFP labels granular cytoplasmic structures at the cell periphery, in both Arabidopsis and Poplar. In contrast, NRAMP3.2-GFP is present on the vacuolar membrane. Images represent vacuolar planes of root epidermal cells (early elongation zone). Transmitted-light (differential interference contrast, *DIC*) and fluorescence (*GFP)* acquisitions are shown. Scale bar : 10 µm.

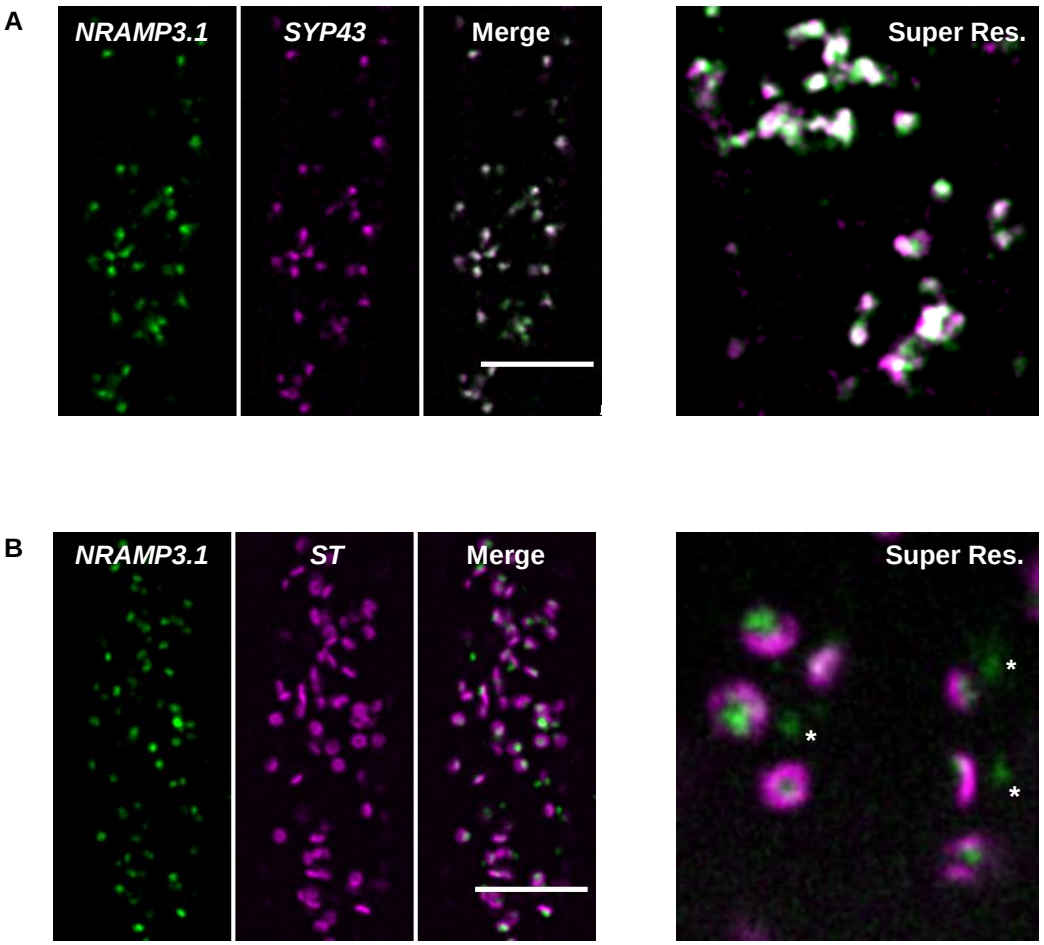

Fig. 9. PotriNRAMP3.1-GFP localizes to the Trans-Golgi Network (TGN) compartment. (A) Colocalisation of PotriNRAMP3.1-GFP with the TGN marker mRFP-SYP43. (B) Juxtaposition of PotriNRAMP3.1-GFP with the trans-Golgi apparatus marker mRFP-ST. Note how PotriNRAMP3.1-GFP signal either faces the center of the toroidal structure of the trans-Golgi or is present as Golgi-independent structures (white asterisks). On the merged images the overlap of GFP (green) and mRFP (magenta) channels appears white. Spinning disk confocal images were acquired in the cortical planes of root epidermal cells in the early elongation zone of Arabidopsis F1 seedlings. Scale bar : 10 µm. Super resolution acquisitions (*Super Res.*) are 10 µm wide.

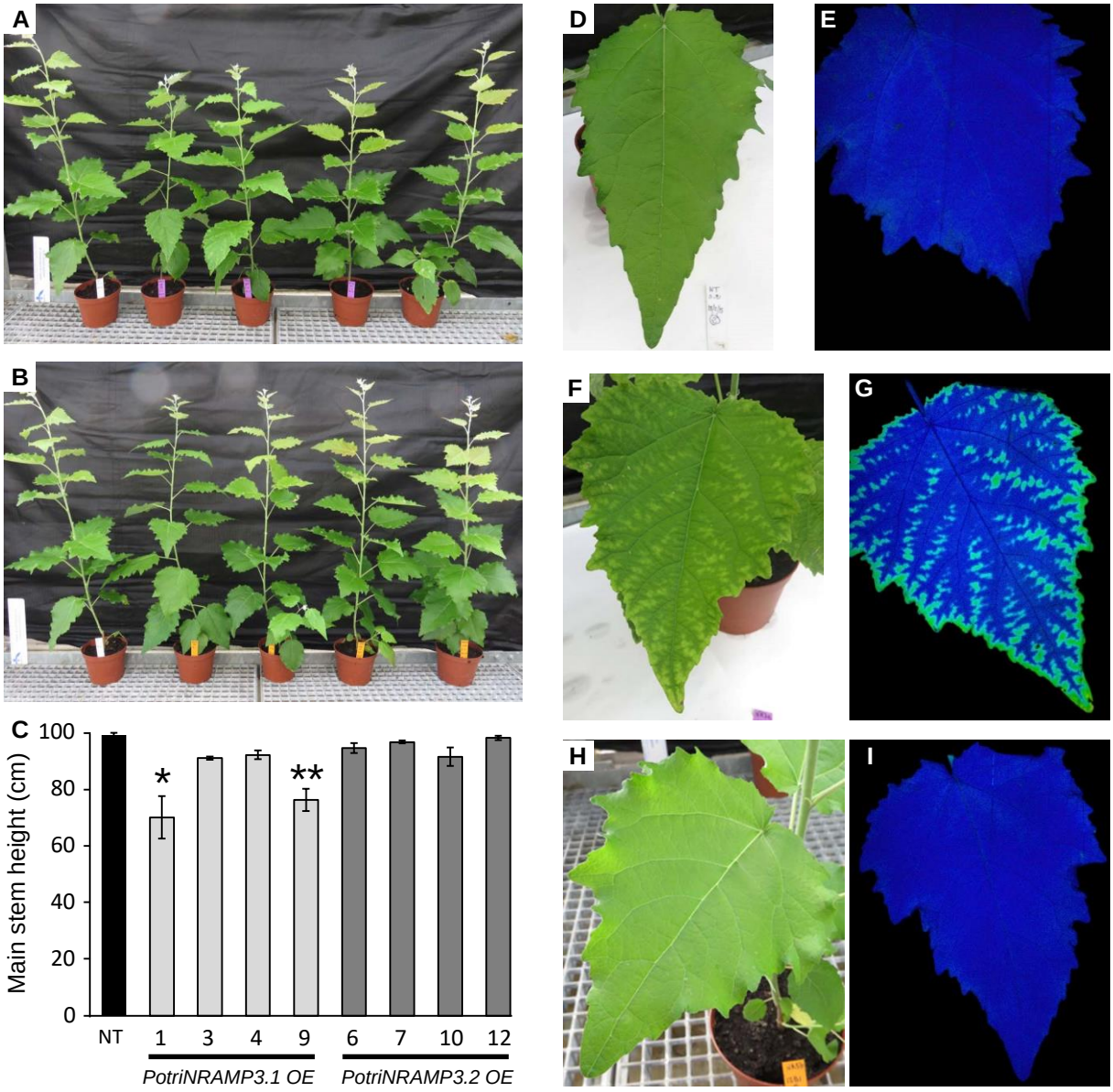

Fig. 10. The ectopic over expression of *PotriNRAMP3.1* but not that of *PotriNRAMP3.2* leads to phenotypic alterations in poplar. Overview of transgenic poplar expressing *PotriNRAMP3.1-GFP* (A, purple tags) or *PotriNRAMP3.2-GFP* (B, orange tags) along with NT control (A and B, white tag), 2 months after transfer from *in vitro* to soil. (C) Mean heights of poplar from the different genotypes. Error bars represent SE (n = 4-7). Asterisks denote significant difference with respect to NT control according to a Mann-Whitney test (*: $p < 0.05$, **: $p < 0.01$). (D-I) Leaf phenotypes of representative trees. (D,E) NT control, (F,G) PotriNRAMP3.1-GFP line 9 (H,I) PotriNRAMP3.2-GFP, line 12. (D, F, H) pictures; (E, G, I) PS II maximum quantum yield measured with imaging Pulse-Amplitude-Modulation. Relative *PotriNRAMP3.1* and *PotriNRAMP3.2* mRNA levels of over-expressing lines are shown in supplementary figure S11.

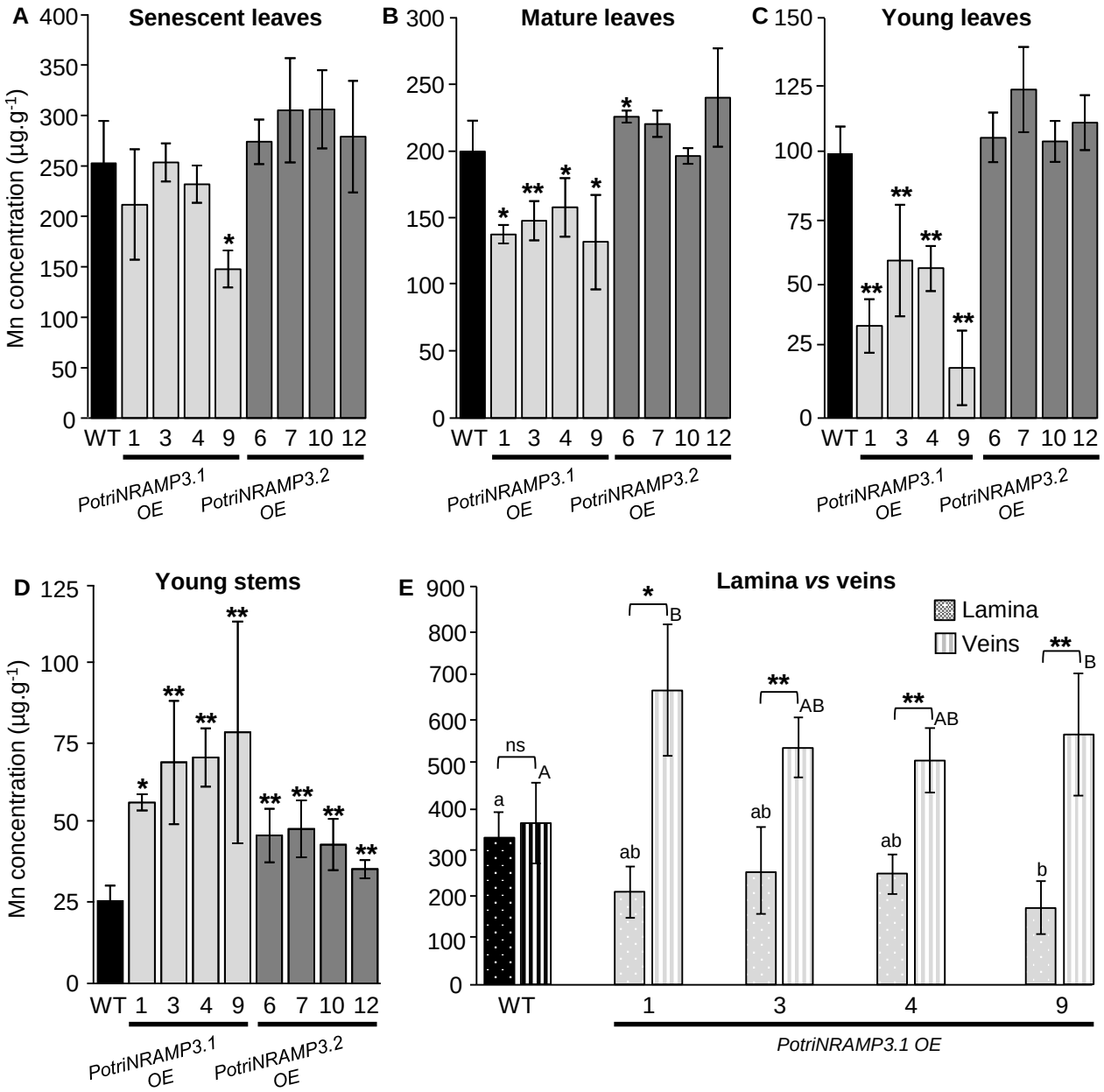

Fig. 11. Ectopic over expression of *PotriNRAMP3.1-GFP* but not that of *PotriNRAMP3.2-GFP* perturbs Mn distribution in poplar leaves. Mn concentrations in senescent (A), mature (B), young leaves (C) and young stems (D) of poplars 2 months after transfer from *in vitro* to soil were determined using Atomic Emission Spectroscopy. Mean Mn concentrations of PotriNRAMP3.1-GFP or PotriNRAMP3.2-GFP OE lines were compared with NT control. Error bars represent SD (n = 4-7). Asterisks denote significant differences with the NT control according to a Mann-Whitney test (*: $p < 0.05$, **: $p < 0.01$). (E) Mean Mn concentrations in veins and lamina of leaves from NT control and 4 *PotriNRAMP3.1-GFP* OE lines. Error bars represent SD (n = 3-6). Asterisks denote significant differences between veins and lamina according to a Mann-Whitney test (*: $p < 0.05$, **: $p < 0.01$). Different letters denote significant differences among genotypes in the lamina (lowercase) or in the veins (capitals) according to a Kruskal-Wallis test followed by Dunn's test for multiple comparison ($p < 0.01$).

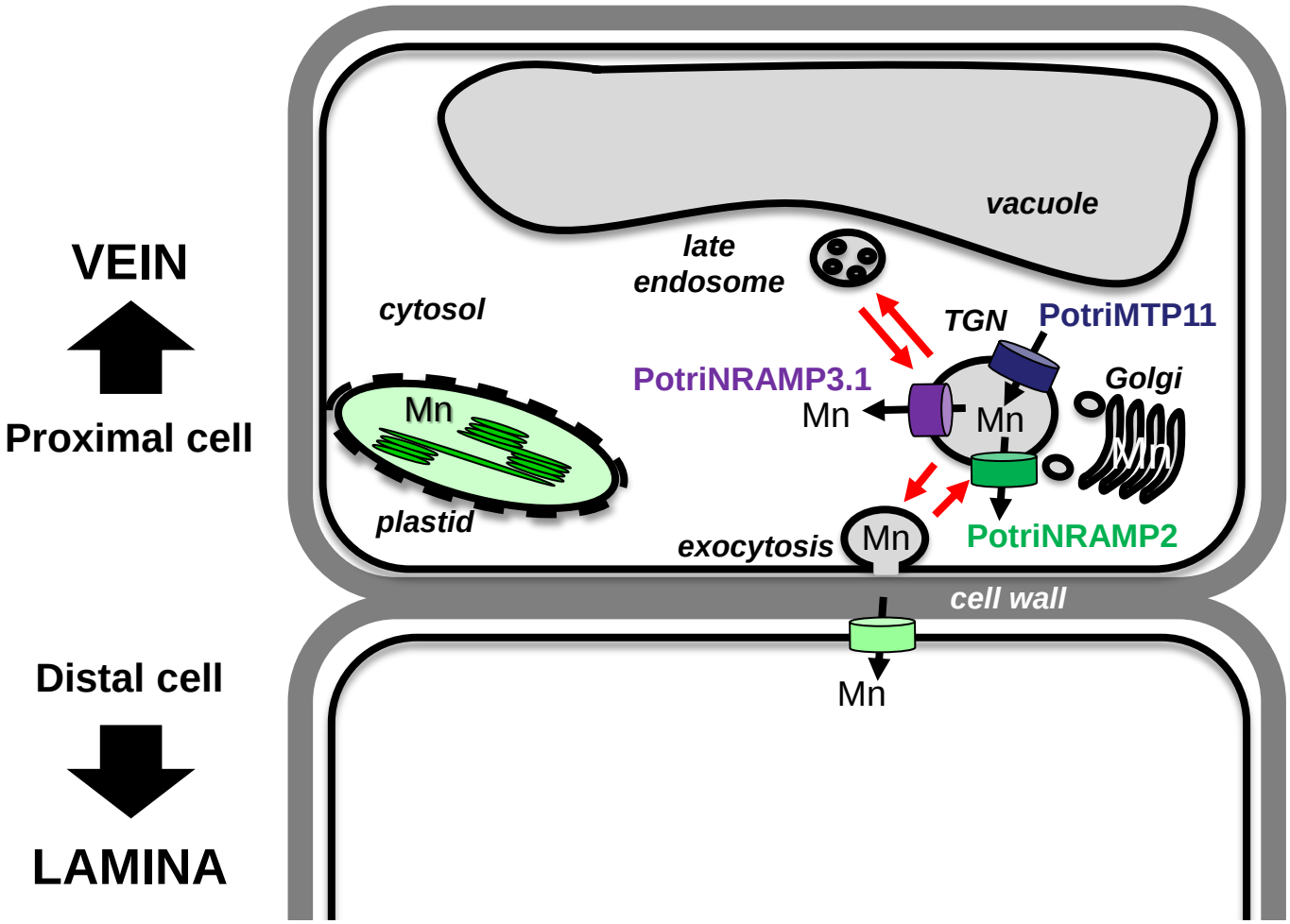

Fig. 12. Working model to account of PotriNRAMP3.1 role in Mn transport from cell to cell. The model is based on the hypothesis that Mn moves through the transcellular pathway, being secreted in the apoplast via exocytosis by the cells proximal to the veins and taken up by the cells that are distal to the veins. According to this hypothesis, the transporters loading Mn (PotriMTP11) or unloading Mn (PotriNRAMP3.1 as well as PotriNRAMP2 assuming function conservation with Arabidopsis AtNRAMP2) from the secretory pathway would determine the amount of Mn made available by proximal cells for uptake by distal cells. In this context, efficient removal of Mn from the secretory pathway in the proximal cells by PotriNRAMP3.1 overexpression would limit Mn availability for the distal cell.